Sinan GENÇ

A Ph.D. Thesis

AGU 2023

PARTICLE SENSING USING OPTICAL NEURAL NETWORKS

A THESIS
SUBMITTED TO
THE DEPARTMENT OF
ELECTRICAL AND COMPUTER ENGINEERING AND
THE GRADUATE SCHOOL OF ENGINEERING & SCIENCE
OF ABDULLAH GUL UNIVERSITY
IN PARTIAL FULFILLMENT OF THE REQUIREMENTS
FOR THE DEGREE OF
Ph.D.

By
Sinan GENÇ
June 2023

PARTICLE SENSING USING OPTICAL NEURAL NETWORKS

A THESIS
SUBMITTED TO
THE DEPARTMENT OF
ELECTRICAL AND COMPUTER ENGINEERING AND
THE GRADUATE SCHOOL OF ENGINEERING & SCIENCE
OF ABDULLAH GUL UNIVERSITY
IN PARTIAL FULFILLMENT OF THE REQUIREMENTS
FOR THE DEGREE OF
Ph.D.

By
Sinan GENÇ
June 2023

SCIENTIFIC ETHICS COMPLIANCE

I hereby declare that all information in this document has been obtained in accordance with academic rules and ethical conduct. I also declare that, as required by these rules and conduct, I have fully cited and referenced all materials and results that are not original to this work.

Sinan GENÇ

REGULATORY COMPLIANCE

Ph.D. thesis titled “Particle Sensing Using Optical Neural Networks” has been prepared in accordance with the Thesis Writing Guidelines of the Abdullah Gül University, Graduate School of Engineering & Science.

Prepared By	Advisor	Co-Advisor
Sinan GENÇ	Assoc. Prof. Kutay İÇÖZ	Assist. Prof. Talha ERDEM

Head of the Electrical and Computer Engineering Program

Assoc. Prof. Zafer AYDIN

ACCEPTANCE AND APPROVAL

Ph.D. thesis titled “Particle Sensing Using Optical Neural Networks” and prepared by Sinan Genç has been accepted by the jury in the Electrical and Computer Engineering Graduate Program at Abdullah Gül University, Graduate School of Engineering & Science.

12/06/2023

JURY:

Advisor : Assoc. Prof. Kutay İÇÖZ…….....

Member : Prof. Mehmet ŞAHİN……..…….…….....

Member : Assist. Prof. Dooyoung HAH…….....

Member : Prof. Hümeyra ÇAĞLAYAN ……..…….....

Member : Doç. Dr. İbrahim Tuna ÖZDÜR …….…….....

APPROVAL:

The acceptance of this Ph.D. thesis has been approved by the decision of the Abdullah Gül University, Graduate School of Engineering & Science, Executive Board dated ….. /….. / …….. and numbered ……..……. .

…….. /…….. / ……..

Graduate School Dean
Prof. İrfan ALAN

ABSTRACT

PARTICLE SENSING USING OPTICAL NEURAL NETWORKS

Sinan GENÇ
Ph.D. in Electrical and Computer Engineering

Advisor: Assoc. Prof. Kutay İÇÖZ
Co-Advisor: Assist. Prof. Talha ERDEM

June 2023

Microplastics are tiny plastic particles that are less than 5mm in length. They are often found in oceans, rivers, lakes, and even the atmosphere, as a result of plastic pollution. The problem with microplastics is that they can have negative impacts on the environment and the organisms living in it. Furthermore, microplastics can also release toxic chemicals into the environment, which can harm aquatic life and even humans. The accumulation of microplastics can also have detrimental effects on the food chain, as smaller organisms are consumed by larger organisms.

To address the problem of microplastics, researchers have developed different detection methods. One common method is the use of spectroscopic techniques such as Fourier transform infrared spectroscopy (FTIR) and Raman spectroscopy. These techniques can identify the chemical composition of microplastics, which can help determine their sources and potential impacts. Another method is the use of microscopy, which allows for the visualization and counting of microplastics in samples.

In this study, we aimed a cost-effective, portable, and simple device to detect and classify microplastics in terms of their size and refractive index. In addition, concentrations can be determined using calibration curves defined for the experimental setup. The main contribution to the literature is identification of two same-sized sphere-shaped microplastics which are made up form two different material. So, in addition to size or shape classification, it will be possible to determine material types with this setup using optical scattering patterns which are dependent of refractive index.

Keywords: scattering, optics, sensing, microparticle, machine learning.

ÖZET

OPTİK SİNİR AĞLARI KULLANARAK PARÇACIK ALGILAMA

Sinan GENÇ
Elektrik ve Bilgisayar Mühendisliği Anabilim Dalı Doktora

Danışman: Doç. Dr. Kutay İÇÖZ
İkinci Danışman: Dr. Öğr. Üyesi Talha ERDEM

Haziran 2023

Mikroplastikler, 5mm'den daha kısa olan küçük plastik parçacıklarıdır. Okyanuslar, nehirler, göller ve hatta atmosferde plastik kirliliği sonucu bulunurlar. Mikroplastiklerin problemi, çevre ve içinde yaşayan organizmalar üzerinde olumsuz etkilere sahip olabilecekleridir. Ayrıca, mikroplastikler, toksik kimyasalların çevreye salınmasına da neden olabilir, bu da sucul yaşamı hatta insanları bile zararlı etkileyebilir. Mikroplastik birikimi, daha küçük organizmaların daha büyük organizmalar tarafından tüketilmesiyle besin zincirinde zararlı etkilere neden olabilir.

Mikroplastiklerin probleminin çözümü için, araştırmacılar farklı tespit yöntemleri geliştirmişlerdir. Yaygın bir yöntem, Fourier dönüşümlü kızılötesi spektroskopisi (FTIR) ve Raman spektroskopisi gibi spektroskopik tekniklerin kullanımıdır. Bir diğer yöntem, mikroskopi kullanımıdır, bu, örnekteki mikroplastiklerin görselleştirilmesine ve sayılmasına olanak tanır. Ayrıca, bazı araştırmacılar, midyeler ve solucanlar gibi organizmaları kullanarak çevredeki mikroplastik varlığını tespit etmek için biyolojik yöntemler geliştirmişlerdir.

Bu çalışmada, mikroplastikleri boyutlarına ve kırılma indislerine göre tespit etmek ve sınıflandırmak için maliyet etkin, taşınabilir ve basit bir cihaz geliştirmeyi amaçladık. Ayrıca, deney kurulumu için tanımlanan kalibrasyon eğrileri kullanılarak konsantrasyonlar belirlenebilir. Literatüre katkımız, iki farklı malzemeden oluşan aynı boyutta küre şeklindeki mikroplastiklerin tanımlanmasıdır. Böylece, boyut veya şekil sınıflandırmasına ek olarak, bu kurulum kullanılarak kırılma indisi bağımlı optik saçılma desenleri kullanılarak malzeme tiplerinin belirlenmesi mümkün olacaktır.

Anahtar kelimeler: saçılma, optik, algılama, mikro-parçacık, makina öğrenmesi.

Acknowledgements

Thanks to my family, advisors, friends, I’M NOT A BARISTA, Konrad Adenauer Stiftung, Global Solutions Initiative, IEEE Photonics Society, and Coffee Manifesto.

TABLE OF CONTENTS

LIST OF FIGURES

LIST OF TABLES

LIST OF ABBREVIATIONS

DLS	Dynamic light scattering
FTIR	Fourier-transform infrared spectroscopy
MALS	Multi-angle light scattering
Me	Melamine
PS	Polystyrene
SDG	Sustainable development goal
SEM	Scanning electron microscopy
SLS	Static light scattering
UPW	Ultra-Pure water

“To infinity and beyond"

Chapter 1

Introduction

1.1 Microplastic Pollution

Microplastics are tiny pieces of plastic that are less than 5mm in length. They come from various sources such as broken-down plastic waste, microbeads from personal care products, synthetic fibers from textiles, and through fragmentation of larger plastic debris [1–3]. Microplastics pose a significant threat to marine and freshwater ecosystems as they are frequently ingested by aquatic life and can accumulate in the food chain, ultimately reaching humans [4–9]. As given in Fig.1.1, micrometer-size living beings in the oceans have plastics in their body [10,11]. Other life forms which are at higher places in food chain, consume them and thus, micro pollutants reach to human body.

Figure 1.1 (a) A zooplankton (2-20 µm), and (b) a water flea (200+ µm) with microplastics in their body.

Plastics from automobile tires, industry, and other resources enhanced the amount of those pollutants in addition to this aquatic connection [12–16]. Recent scientific studies have demonstrated the presence of these tiny particles in the bodies, blood, milk, and flesh of farm animals, as well as in food products including honey, sugar, salt, and seafood.

Another study indicated that micro/nanosized submerged plastics rise to the surface of the water and mix with the air as a result of evaporation [17]. Rains return microplastics in the air to the earth, making contact, even breathing them inevitable. The danger of breathing in microplastics increases with their smaller size [18]. In Fig. 1.2, a sample

cycle to the microplastic pollution is given [19]. Pollutants from daily life activities. reach to the water sources, seas, and oceans. Mechanical, biological, or natural process make them smaller and complete the cycle with sea food, atmosphere or direct water consuming.

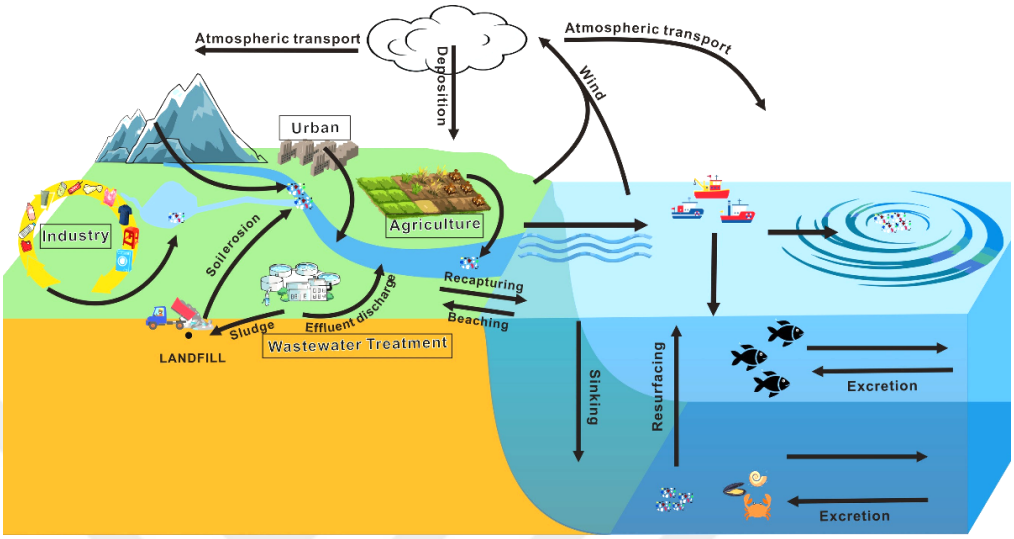

Figure 1.2 A sample microplastic pollution cycle example.

The environmental impacts of microplastics are still not completely understood, but they have been linked to health problems in marine life, such as reproductive issues, behavioral changes, and death. In addition, microplastics can also have economic impacts on fishing and tourism industries as the presence of plastic in water can reduce fish populations and lead to beach closures [20].

The issue of microplastics has gained attention in recent years due to the increasing amount of plastic waste being produced globally [21–24]. Plastic is cheap, versatile, and durable, but it is also non-biodegradable, and as a result, it can persist in the environment for centuries. the environment is to reduce the use of plastic and increase awareness of the issue.

Recent years have seen an increase in research on microplastic pollution, with numerous studies highlighting the extent of the problem. In 2018, a study estimated that microplastics were present in more than 90% of bottled water, with an average of 325 particles per liter [25]. A separate study published in 2020 estimated that up to 14 million metric tons of microplastics were deposited in the world's oceans each year, with the majority originating from Asia [26]. Additionally, a study published in 2023 found that microplastics were present in more than 90% of the freshwater samples collected from the Amazon and its tributaries [27]. These findings highlight the urgent need for action to

address the root causes of microplastic pollution and to prevent further harm to our environment and health.

Figure 1.3 A sample map for microplastics and their detected locations around the world.

As microplastics are so small, it is difficult to remove them from the environment once they have been released, and current recycling efforts are not effective in eliminating them. In Fig. 1.3, some of microplastics and their locations are presented [28]. Therefore, the best way to prevent microplastics from entering Some measures being taken to address the problem include the introduction of legislation to ban microbeads in personal care products, the promotion of sustainable alternatives, and increased investment in research to better understand the impacts of microplastics on the environment and human health.

1.2 Detection of Microplastics

Microplastics detection by optical scattering is a technique that uses light scattering to identify and quantify microplastic particles in a sample. The technique relies on the fact that microplastics are usually small enough to scatter light at a particular angle, allowing them to be distinguished from other particles in the sample.

To perform microplastics detection by optical scattering, a sample is first prepared by filtering it through a fine mesh or membrane to remove larger particles. The filtered sample is then passed through a laser beam or other light source that is directed at a specific angle to the sample. As the light passes through the sample, it interacts with any

microplastic particles present, causing them to scatter light at a particular angle. A detector is positioned to capture this scattered light, which can then be analyzed to identify and quantify the microplastics in the sample.

One advantage of this technique is that it is non-destructive and non-invasive, meaning that the sample can be preserved for further analysis if needed. Additionally, it can be performed relatively quickly and requires minimal sample preparation.

However, microplastics detection by optical scattering does have some limitations. For example, it may not be able to detect very small microplastics or those that are transparent or translucent. In addition, other particles in the sample may also scatter light, which can make it difficult to distinguish microplastics from other particles. Therefore, it is often used in combination with other analytical techniques, such as microscopy or spectroscopy, to provide a more complete picture of the microplastics present in a sample. There are several optical techniques that can be used to detect microplastics in various environmental samples, such as sediment, soil, and air. Some of the most common optical techniques used for microplastic detection are:

Fluorescence microscopy: This technique involves labeling microplastics with a fluorescent dye and then visualizing them under a microscope with a UV light source. The microplastics appear as bright fluorescent particles against a dark background, making them easy to detect and quantify.

Fourier-transform infrared (FTIR) spectroscopy: FTIR spectroscopy is a technique that measures the absorption or transmission of infrared light by a sample. Different types of plastic have unique infrared spectra, which can be used to identify and quantify microplastics.

Hyperspectral imaging: Hyperspectral imaging involves collecting images at multiple wavelengths across the electromagnetic spectrum, allowing for the identification and characterization of microplastics based on their spectral signatures.

Digital holographic microscopy: Digital holographic microscopy is a technique that involves recording interference patterns generated by a laser beam that has passed through a sample. This technique can be used to detect and characterize microplastics based on their 3D morphology and optical properties.

Within the framework of this thesis, optical techniques can be used to determine microplastics in liquids, such as water, by either visualizing the microplastics directly or indirectly detecting them through their interaction with light. Some of the most commonly used optical techniques for determining microplastics in liquids are:

Microscopy: Microscopy techniques, such as brightfield, darkfield, and phase contrast microscopy, can be used to directly visualize microplastics in liquid samples. Fluorescence microscopy can also be used if the microplastics are labeled with a fluorescent dye.

Flow cytometry: Flow cytometry is a technique that can be used to quantify and size particles in a liquid sample. Microplastics can be labeled with a fluorescent dye and then analyzed by flow cytometry to determine their concentration and size distribution.

Infrared spectroscopy: Infrared spectroscopy can be used to identify and quantify microplastics in liquid samples by measuring their characteristic absorption or transmission of infrared light.

Raman spectroscopy: Raman spectroscopy is a non-destructive technique that involves shining a laser on a sample and measuring the scattered light. Each type of plastic has a unique Raman spectrum, which can be used to identify and quantify different types of microplastics.

Surface plasmon resonance imaging: Surface plasmon resonance imaging can be used to detect and quantify microplastics in liquid samples based on their interaction with a metallic surface. The presence of microplastics in the liquid sample causes changes in the refractive index of the surrounding medium, which can be detected by surface plasmon resonance imaging.

Overall, optical techniques provide powerful tools for detecting and characterizing microplastics in various environmental samples and can be used to generate important data for monitoring and mitigating microplastic pollution.

1.3 Contributions and Structure of Thesis

In literature, there are studies to distinguish particles at different size regardless of the material. It is easier to classify particles at different size. However, if the particles are exactly same in every aspect but the materials they made of, that situation would be tricky. In this thesis, in addition to the particle size, concentration and incident wavelength, the materials of particles are also examined and classification by random forest algorithm is presented. Distinguishing the particle will open a new window to classify microplastic pollution in terms of their danger level and track their path starting from the source. Thus, it will be possible to take precautions at the beginning. As it was stated before, it is difficult to eliminate those particles once they already distributed to the environment.

In first experiments, as presented in Fig 1.4 by unprofessional photos by mobile, it was clearly observed that a low-cost setup is able to show different scattering patterns for particles at different size, refractive index, concentration, and incident wavelength.

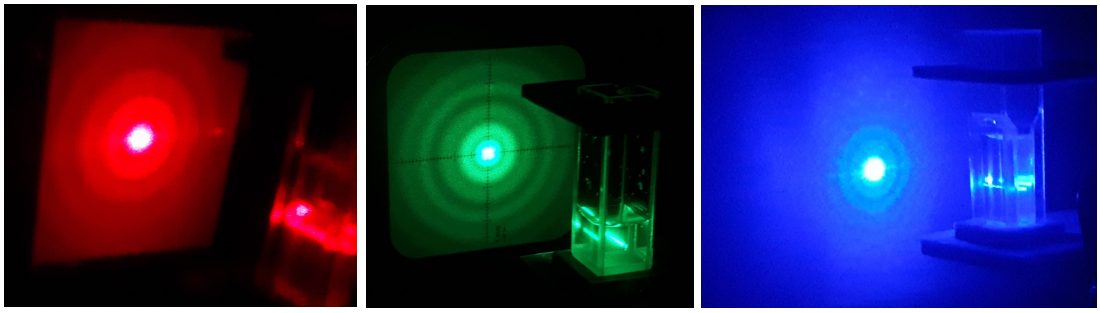

Figure 1.4 Mobile phone shooting to show different patterns meaning that proposed low-cost setup would provide information for classification.

In this thesis, the theory of scattering, derivations and proposed system is given in Chapter 2. Then, in Chapter 3, experimental setup, samples, image processing and machine learning steps are explained. Chapter 4 includes the effect of parameters i.e., concentration, particle size, particle refractive index, and incident wavelength on scattering. Machine learning integration and results are given in Chapter 5. At the end, thesis finishes with Chapter 6, conclusions, prospects, societal and sustainable contributions.

Chapter 2

Background

2.1 Derivation of Mie Theory

Mie scattering theory is a theoretical framework that describes the scattering of electromagnetic radiation by particles that are comparable in size to the wavelength of the radiation. This type of scattering is named after the German physicist Gustav Mie, who first developed the theory in 1908. The Mie theory is an extension of Rayleigh scattering theory, which is valid for particles much smaller than the wavelength of the radiation. Mie scattering theory is particularly relevant in the study of atmospheric and oceanic optics, as well as in the field of materials science.

Mie scattering is a theoretical model that describes the scattering of light by spherical particles, such as dust, water droplets, and biological cells. While Mie scattering is a powerful tool for understanding light scattering in many physical and biological systems, there are several limitations to the model that should be considered:

Size and shape: Mie scattering is only applicable to spherical particles with a uniform refractive index. If the particles are not spherical, or if their refractive index is not uniform, Mie scattering may not accurately describe the scattering behavior.

Size parameter: Mie scattering is most accurate for particles whose size is much larger than the wavelength of light being scattered. For particles that are smaller than the wavelength of light, or larger than several wavelengths, Mie scattering may not be a good approximation.

Homogeneity: Mie scattering assumes that the medium in which the particles are suspended is homogeneous and isotropic. If the medium is not homogeneous, or if there are gradients in the refractive index or density, Mie scattering may not provide an accurate description of the scattering behavior.

Multiple scattering: Mie scattering assumes that the scattered light only undergoes a single scattering event. In reality, light can undergo multiple scattering events, which can cause deviations from the Mie scattering predictions.

In Mie scattering theory, the scattered light is not uniformly distributed in all directions, as is the case in Rayleigh scattering. Instead, the scattered light is concentrated in a number of specific directions, known as Mie resonances. These resonances are determined by the size and refractive index of the scattering particle, as well as the wavelength of the incident radiation. Mie scattering theory provides a mathematical framework for calculating the intensity and polarization of the scattered light as a function of these parameters. The theory has applications in a wide range of fields, including meteorology, remote sensing, and the design of optical devices.

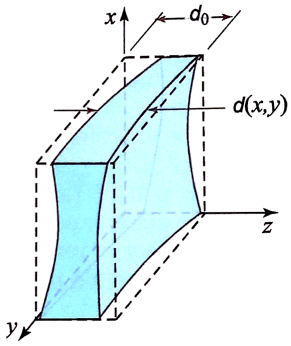

Figure 2.1 Variable-thickness plate as starting point of derivations.

The derivation of Mie scattering equations start from a variable-thickness plate concept as given in Fig. 2.1.

$$t(x,y) \sim exp\left[-j(n-1)\,2d(x,y)\right] \tag{2.1}$$

For spheres

$$d(x,y) = 2\sqrt{R^2-\left(x^2+y^2\right)} \tag{2.2}$$

Free-space propagation (Fourier transform in far-field)

$$g(x,y) \sim F\left(\frac{x}{\lambda d},\frac{y}{\lambda d}\right) \tag{2.3}$$

2D intensity matrix (image)

$$I(x,y) \sim \frac{1}{(\lambda d)^2}\left|T\left(\frac{x}{\lambda d},\frac{y}{\lambda d}\right)\right|^2 \tag{2.4}$$

As presented in Eq. 4, 2D Fourier transformation makes hand calculations difficult to deal with. Thus, solvers needed to obtain scattering patterns as theoretical results.

In Mie Theory, differential scattering cross-sections (i_1, i_2) are defined as given in Eq. (5) and Eq. (6) for vertically and horizontally polarized incident and scattered light.

$$i_1 = \left| \sum_{n=1}^{\infty} \frac{2n+1}{(n(n+1)} [a_n \pi_n(cos\theta) + b_n \tau_n(cos\theta)] \right|^2 \tag{2.5}$$

$$i_2 = \left| \sum_{n=1}^{\infty} \frac{2n+1}{(n(n+1)} [a_n \tau_n(cos\theta) + b_n \pi_n(cos\theta)] \right|^2 \tag{2.6}$$

where τ_n and π_n express Legendre polynomials in Eq. (7) and Eq. (8),

$$\pi_n(cos\theta) = \frac{P_n^{(1)}(cos\theta)}{sin\theta} \tag{2.7}$$

$$\tau_n(cos\theta) = \frac{dP_n^{(1)}(cos\theta)}{d\theta} \tag{2.8}$$

and where parameters a_n and b_n are defined as given in Eq. (9) and Eq. (10).

$$a_n = \frac{\Psi_n(\alpha)\Psi_n'(m\alpha) - m\Psi_n(m\alpha)\Psi_n'(\alpha)}{\xi(\alpha)\Psi_n'(m\alpha) - m\Psi_n(m\alpha)\xi_n'(\alpha)} \tag{2.9}$$

$$b_n = \frac{m\Psi_n(\alpha)\Psi_n'(m\alpha) - \Psi_n(m\alpha)\Psi_n'(\alpha)}{m\xi(\alpha)\Psi_n'(m\alpha) - \Psi_n(m\alpha)\xi_n'(\alpha)} \tag{2.10}$$

Size parameter, α, is defined by

$$\alpha = \frac{2\pi a m_o}{\lambda_o} \tag{2.11}$$

where m_o is the refractive index of the medium, λ_o is incident wavelength respect to vacuum and m is the refractive index of the particle itself. The Ricatti-Bessel functions, Ψ, and ξ are defined by the half-integer-order Bessel function of the first kind, where

$$\Psi_n(z) = \left(\frac{\pi z}{2}\right)^{\frac{1}{2}} J_{n+1/2}(z) \tag{2.12}$$

$$\xi_n(z) = \left(\frac{\pi z}{2}\right)^{\frac{1}{2}} H_{n+1/2}(z) = \Psi_n(z) + i\mathrm{X}_n(z) \tag{2.13}$$

$H_{n+1/2}(z)$ is the half-integer-order Hankel function of the second kind and $\mathrm{X}_n(z)$ is defined by half-integer-order Bessel function of second kind ($Y_{n+1/2}(z)$),

$$\mathrm{X}_n(z) = -\left(\frac{\pi z}{2}\right)^{\frac{1}{2}} Y_{n+1/2}(z) \tag{2.14}$$

After all those steps, differential scattering cross sections (i_1, i_2) are calculated and average of them represents the randomly polarized (unpolarized) incident and scattered light cross section.

Overall, while Mie scattering is a useful tool for understanding light scattering by spherical particles, its limitations should be considered when applying the model to real-world systems.

2.2 How to Measure Scattering?

Scattering theory is a fundamental concept in physics that describes the behavior of waves and particles when they interact with a potential or obstacle. It is a branch of quantum mechanics that plays a crucial role in understanding the properties of matter and energy at the atomic and subatomic level. Scattering theory provides a mathematical framework to calculate the probability of a particle being scattered in a particular direction, as well as the phase shift of the scattered wave. It has applications in a variety of fields, including nuclear physics, solid-state physics, astrophysics, and even in medical imaging. In this context, understanding scattering theory is essential for anyone interested in exploring the behavior of waves and particles at the quantum level.

There are several types of scattering, each characterized by the nature of the incident wave and the target or scatterer involved. The most common types of scattering include:

Rayleigh Scattering: This type of scattering occurs when electromagnetic radiation, such as visible light or radio waves, interacts with particles that are much smaller than the wavelength of the radiation. Rayleigh scattering is responsible for the blue color of the sky, as well as the reddening of the sun at sunset.

Mie Scattering: Mie scattering occurs when electromagnetic radiation interacts with particles that are comparable in size to the wavelength of the radiation. This type of scattering is responsible for the white color of clouds, as well as the colors of certain gemstones.

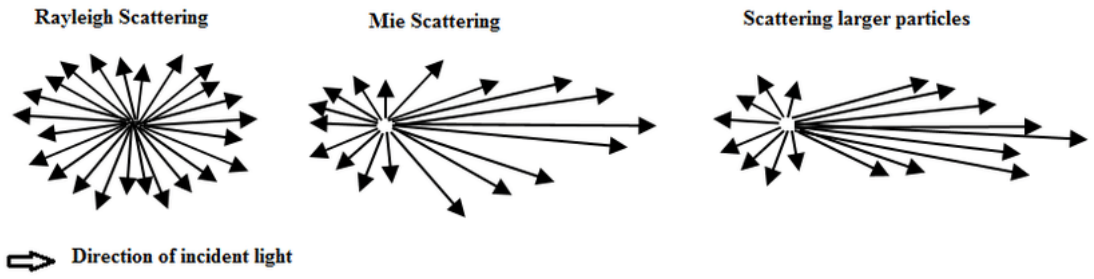

Figure 2.2 Optical scattering intensity levels at different angles dependent on particle size.

As presented in Fig. 2.2, when particle size gets bigger, forward scattering gets dominant [29]. Scattered light around zero-degree gets closer to the zero degree and make a brighter and smaller spot on the screen.

Compton Scattering: Compton scattering occurs when high-energy photons, such as X-rays or gamma rays, collide with charged particles, such as electrons. During this process, the photon loses energy and changes direction.

Rutherford Scattering: Rutherford scattering occurs when charged particles, such as alpha particles, interact with the nucleus of an atom. During this process, the trajectory of the charged particle is deflected due to the electrostatic repulsion between the two charged particles.

Elastic Scattering: Elastic scattering occurs when the energy and momentum of the incident particle are conserved during the scattering process. This type of scattering is characterized by a change in direction of the incident particle, without any change in its energy or wavelength.

Inelastic Scattering: Inelastic scattering occurs when the energy and momentum of the incident particle are not conserved during the scattering process. This type of scattering is characterized by a change in energy, wavelength, or both, of the incident particle.

Scattering theory can be used to detect microplastics in water by analyzing the way light scatters off the particles. When light passes through a medium, such as water, it interacts with particles in the medium, causing it to scatter in different directions. The scattered light can be measured and analyzed to determine the size and concentration of the particles in the medium. Scattering theory can be used in several ways to detect microplastics in water:

Dynamic Light Scattering (DLS): DLS is a technique that measures the intensity and time-dependence of scattered light from particles in a liquid to determine their size distribution. By analyzing the scattered light from microplastics, their size distribution can be determined.

Static Light Scattering (SLS): SLS is a technique that measures the intensity of scattered light from a sample of known concentration and compares it to a standard curve to determine the concentration of the particles in the sample. This technique can be used to quantify the concentration of microplastics in water.

Multi-Angle Light Scattering (MALS): MALS is a technique that measures the intensity of scattered light from a sample at different angles to determine the size

distribution and concentration of the particles in the sample. This technique can be used to determine the size and concentration of microplastics in water.

In this study, after investigation of settlement and having same scattering angles for different concentrations, we assume that movement of particles does not affect experiments. Therefore, it can be said that minor effects of DLS can be ignored, and the system can be assumed as a SLS concept.

There are several methods that can be used to detect and determine the presence of microplastics in water resources. Some of the commonly used methods are:

Filtration: This method involves passing a water sample through a filter with a pore size of less than 5 micrometers to capture microplastics. The filter can then be visually inspected or analyzed using microscopy to determine the type, size, and concentration of microplastics present.

Spectroscopy: This method uses FTIR or Raman spectroscopy to analyze the chemical composition of microplastics. The microplastics can be extracted from water samples using a solvent and then analyzed using a spectrometer to identify the type of plastic.

Fluorescence microscopy: This method involves staining microplastics with a fluorescent dye and then visualizing them under a fluorescence microscope. This technique can be used to determine the size, shape, and concentration of microplastics present.

Flow cytometry: This method involves using a laser to detect and count microplastics in water samples. The microplastics are first stained with a fluorescent dye and then passed through a flow cytometer, which measures the fluorescence and size of each particle.

It is important to note that each method has its advantages and limitations, and a combination of methods may be needed to obtain accurate and comprehensive data on microplastics in water resources. Additionally, standardization of methods and protocols is necessary to ensure comparability of data across studies.

2.4 Proposed System and Developments

Considering the consistent conditions in the laboratories, huge device dimensions, high costs, maintenance requirements and alignment issues a portable, low-cost, small setups are and will be needed due to rapidly increasing global microplastics problems. As

stated in the introduction chapter, it is urgently needed to take precautions at the origin of those pollutants. Once it is possible to detect and classify those particles, it would be easier to define their source and define global measures to decrease the level of microplastics pollution.

In addition to micro size, with minor adjustments, it is also possible to detect nano size particle with the same setup. A thin lens to focus the list on a much smaller area and look for just couple of particles instead of high concentrations and zoom the images taken at the laboratory would open another window to research on nano plastics.

Furthermore, once the appropriate solvents, concentrations, and incident light are provided, it would be possible to investigate on different type of particles. This point will be stated again as future prospects part of this thesis.

In Fig. 2.3, the illustration of experimental setup is presented. Directing a laser beam onto samples in cuvette through an iris and neutral density filter is the part before scattering occurs. When light hits to the particles in cuvette, it scatters, and the pattern falls onto the screen behind. Having particles at different size, refractive index, concentration and using different incident wavelengths results in different scattering patterns. Thus, by a cost-effective setup, different scattering pattern images are acquired.

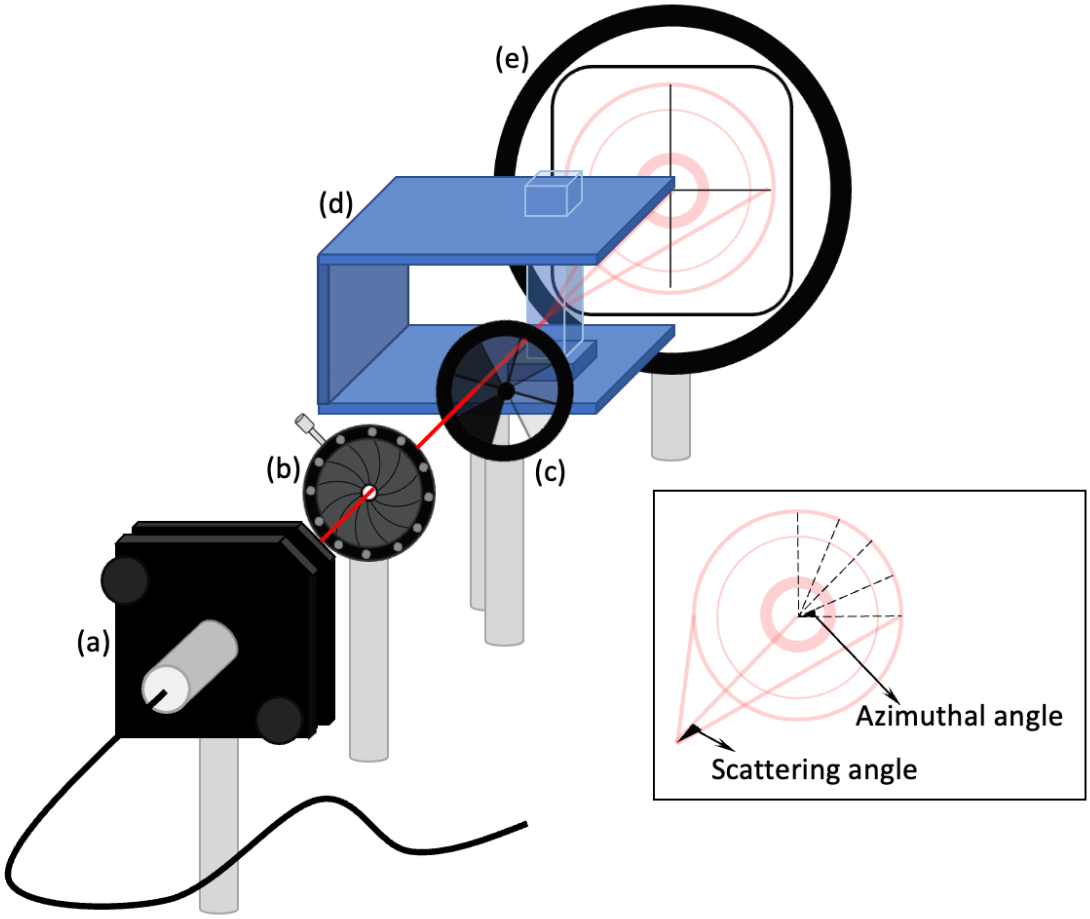

Figure 2.3 Illustration of the experimental setup, (a) light source, (b) iris, (c) neutral density filter, (d) cuvette holder and cuvette, and (e) graded white screen, (inset) azimuthal and scattering angles.

Once the raw images are collected from the setup, we crop them and obtain upper right quartile as in Fig. 2.4(b). This is possible because of having spherical particles which scatter light symmetrically so to decrease computational cost, we work on this quarter only. Next, we convert the image into gray-scale. Comparison of red, green, and blue images in possible when we analyze them in gray version. Then, to get scattering information, we draw azimuthal lines starting from center through outer rings. Again, thanks to symmetry, each line has same pixel values on it. To decrease noise and error, we take the average of the values on those azimuthal line and at the and the scattering information is ready to plot as given in Fig. 2.4(e).

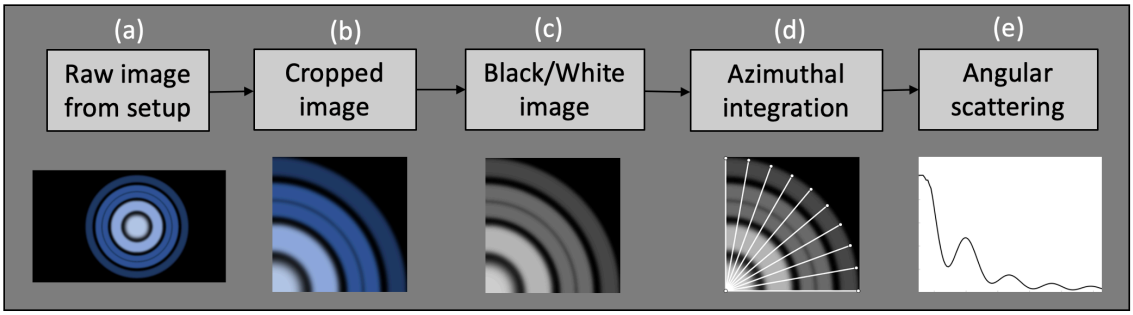

Figure 2.4 Representation of image processing flow from the raw image to scattering pattern.

The peaks on that scattering line represents bright interference rings and the gaps are destructive combinations. Having different samples mean having different patterns and different scattering lines. After all those steps, different sets of peak angles are aimed to use as random forest algorithm inputs.

Chapter 3

Experimental Work

3.1 Sample Preparation

Investigating the impact of material type (particle's refractive index) and particle size is possible using commercially available microparticles made of two different materials, melamine (Me) and polystyrene (PS), at diameters of 8 μm and 10 μm. In order to examine the relationship between particle number and scattering behavior, we also generated samples at various concentrations.

Commercially available 8 μm +/- 100 nm-sized melamine resin (Me8) (95523-Sigma Aldrich), 8 μm +/- 97 nm-sized Polystyrene (PS8) (84192-Sigma Aldrich) and 10 μm +/- 110 nm-sized Polystyrene (PS10) (72986-Sigma Aldrich) microspheres, were used in the experiments to test the match between the predictions of Mie theory that we calculated numerically and the experimental results. Microscope image of Me and PS spheres are given in Fig. 3.1.

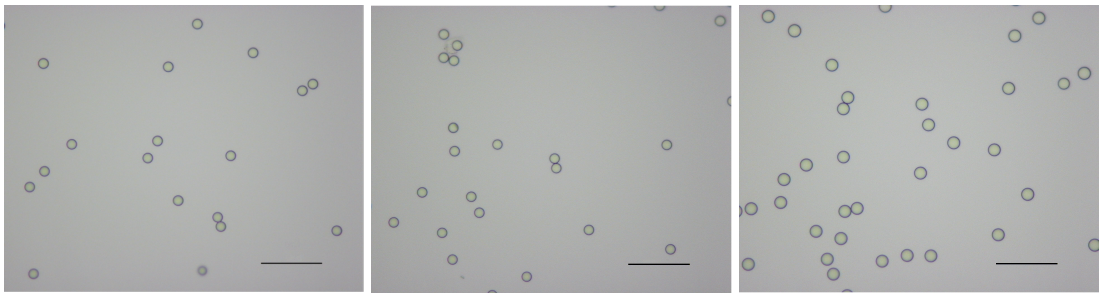

Figure 3.1 40x-zoomed microscope images of (a) Me8, (b) PS8, and (c) PS10 particles. Scale bar: 50 μm.

Samples were prepared at the concentrations from 0.05 fM up to 3.00 fM by adding them into ultra-pure water using a micropipette and kept in vials, Fig. 3.2. The samples were shaken using vortex before the experiments to make the solution much more homogeneous and by hand just before the measurements one more time.

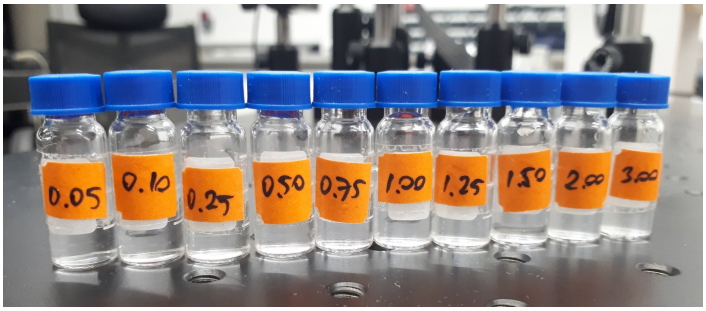

Figure 3.2 Samples prepared at different concentrations.

In our experiments, the safe time limit was about 5 minutes. The sinking of the particles deeper in the cuvette and observation of more than 5% decrease in scattering intensity was observed after 5 minutes. Our measurement time for each sample was much shorter than this limit. In addition, 0.05 - 3.00 fM range corresponds to 3e+4 – 180e+4 particles/mL which is higher than the values studied in the literature. However, the sizes of the particles reported in literature are about 10-100 times bigger, significantly increasing the scattering cross-section. Considering this size difference, we believe that it is reasonable to have 0.05 fM - 3.00 fM concentration range in our experiments for the particle sizes we are interested in [30].

For the refractive index of Melamine particles, there is an uncertainty in the literature. Thus, we studied the range given in literature which is 1.530-1.922 for the red region. The most satisfying match with the Mie theory and experiments were obtained as 1.79 at 656.3 nm. We used refractive indices of 1.89 and 1.96 for 514.9 nm and 403.8 nm, respectively [31–33].

3.2 Experimental Setup

For the measurements, at room temperature (22 ºC), the laser power was kept between 150-170 µW for collimated red, green, and blue lasers emitting light at 403.8 nm, 514.9 nm, and 656.3 nm, respectively (CPS405, CPS520 and CPS650F-THORLABS). The beam was directed through an iris to squeeze the beam radius. Just after the iris, a neutral density filter was used to adjust the laser power to the same level during the experiments. A cuvette holder was 3D printed to keep the cuvette in the optimum orientation and finally a graded white screen was placed to have the scattering pattern on it as presented in Fig. 3.3.

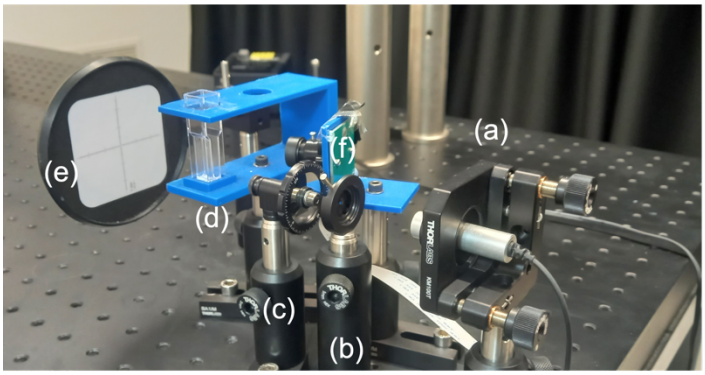

Figure 3.3 Experimental setup, (a) light source, (b) iris, (c) neutral density filter, (d) cuvette holder and cuvette, (e) graded white screen, and (f) camera module.

Subsequently, each sample was placed into cuvettes and the scattering patterns of the laser light at different wavelengths from these particles fell on a screen placed 6.5 cm apart from the cuvette. 200 images of these scattering patterns were taken in a dark environment by a CMOS camera (Raspberry Pi Focus Adjustable Camera Module- 2592x1944 pixels), -100 ms shutter speed and 20 ms exposure time- controlled by Raspberry Pi 4 - 4GB RAM. In total, 1800 images are recorded for processing.

3.3 Image Processing

Having recorded images required following image processing steps to obtain some digital data to be used in machine learning. For each sample, there were 200 images taken, and processing individually was not possible due to high level of noise.

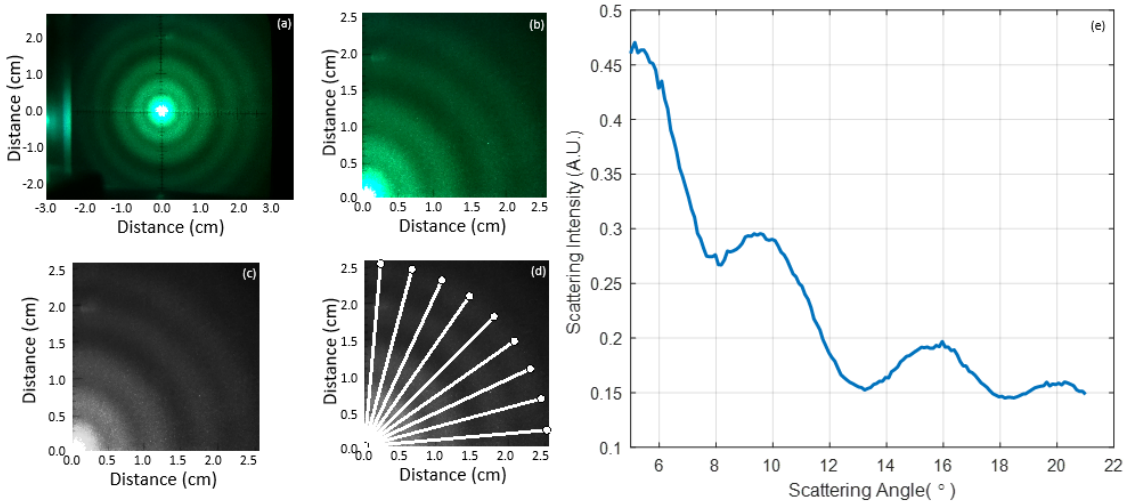

Figure 3.4. (a) Raw scattering image of Me8 particles excited by green laser, (b) cropped image, (c) gray-scale image, (d) data lines on scattering image, (e) average scattering behavior of 86 lines (5º:1º:90º) on 1.50 fM 8 µm Me particles.

The images of the scattering patterns (Fig. 3.4(a)) were analyzed numerically. The average of 200 images was calculated for each sample's scattering pattern to minimize noise. Next, as illustrated in Fig. 3.4(b-c), all the images were cropped and converted to grayscale. To decrease the computational cost, 86 lines were defined with 1º azimuthal angle increments between 5º and 90º starting from the center towards the outer regions on the upper-right quartile of the images as given in Fig. 3.4(d), (Fig. 3.4(d), presents only 10º azimuthal increment for better visualization). As the next step, the average of pixel data on all those 81 lines were taken to decrease the noise level on measurements. Finally, azimuthal angular scattering intensity was obtained as presented in Fig. 3.4(e). However, it was still noisy to identify peak angles so that 2nd degree polynomial was fitted around the peak angles to the experimental data. The scattering angle limit in the light direction is 21º because of the screen size and the distance from the sample.

3.4 Random Forest Algorithm

Random Forest is a popular machine learning algorithm used for both classification and regression tasks. It is an ensemble learning method that creates a set of decision trees and combines their predictions to make a final prediction [34–36].

The algorithm works by first randomly selecting a subset of the data and a subset of the features for each tree in the forest. Then, a decision tree is built using these subsets of data and features. The process is repeated multiple times, resulting in a forest of decision trees as presented in Fig. 3.5 [37].

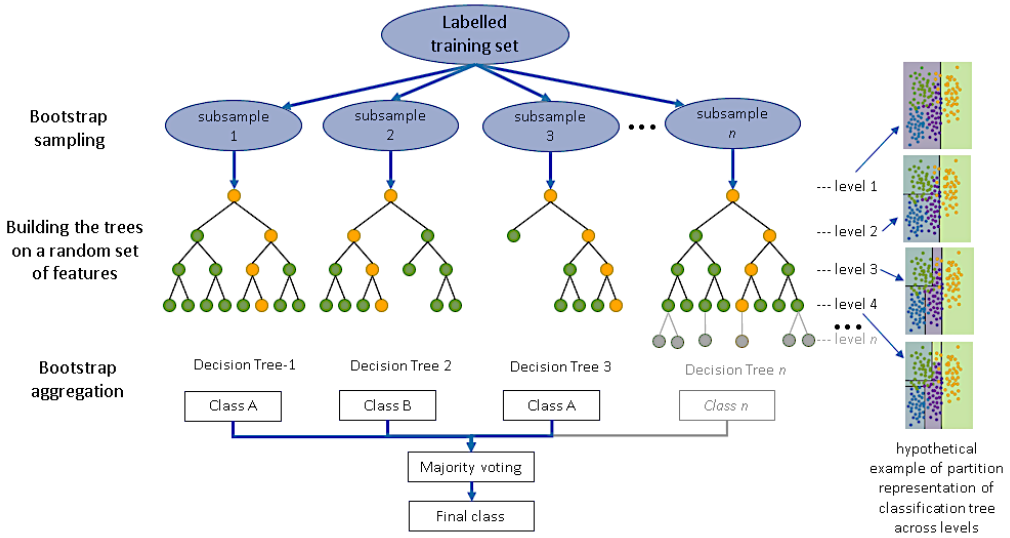

Figure 3.5 Structure of random forest algorithm.

When making a prediction for a new data point, each tree in the forest independently makes a prediction, and the final prediction is made by taking the majority vote of all the trees in the forest.

Random Forest has several advantages over a single decision tree. It is less prone to overfitting, as the individual trees in the forest are trained on different subsets of the data and features. It can handle high-dimensional data and is relatively easy to use, as it requires few hyperparameters to be tuned.

Overall, Random Forest is a powerful and widely used algorithm in machine learning that can be used for a variety of tasks, such as classification, regression, and feature selection.

Given the inherent numerous scatterings of the spheres in liquid, the random forest algorithm offers the opportunity to categorize the measured scattering data, which would not be a simple operation to manage theoretically. Random forest was utilized in this investigation because of its straightforward design and repeatable outcomes. In our earlier study, the correspondence between experimental findings and numerical solutions was revealed. We think that this match made it possible to apply random forest easily in terms of data preparation. This numerical solution methodology produced the data set, which included the incidence wavelength, particle size, material type, and bright ring angles that were used to run the algorithm. A test set of data was created from 20% of all measurements. The remaining part was used to train the random forest algorithm.

Random Forest is a popular machine learning algorithm for classification tasks that works by creating an ensemble of decision trees, where each tree is trained on a subset of the data and a subset of the features. When making a prediction for a new data point, each tree in the forest independently makes a prediction, and the final prediction is made by taking the majority vote of all the trees in the forest. This approach results in a more robust and accurate prediction compared to a single decision tree, as the ensemble of trees can capture the complex interactions and relationships between the features.

One of the main advantages of Random Forest for classification is its ability to handle high-dimensional data. The algorithm can effectively deal with datasets that have a large number of features, where other machine learning algorithms may struggle due to the curse of dimensionality. Additionally, Random Forest is less prone to overfitting compared to other algorithms, as the individual trees in the forest are trained on different subsets of the data and features. This means that the ensemble of trees can capture the general patterns and avoid overfitting to noise in the data. Overall, Random Forest is a

powerful algorithm for classification tasks that can achieve high accuracy and is suitable for a wide range of applications.

The inputs for classifying material types and particle sizes were incident wavelength and bright ring angles. The concentration and scattering intensities were not required for this stage because it was discovered during the image analysis that the peaks were at the same angle for a certain material type and size. However, we are aware that as sphere concentration in samples grew, the total scattering intensity had to rise as well.

Chapter 4

Effects of Particle Size, Concentration, Material, and Incident Wavelength

There are parameters effecting scattering during the investigation of scatterers. Concentration of particles, particle size, refractive index, or the material that particles made of, and incident wavelength. In this chapter, effects of those parameters will be investigated and their relevance to this study will be discussed. Experimental and theoretical results will be given. For theoretical results, equations were embedded on a MATLAB code, and it is given in Appendix A.

4.1 Effect of Concentration on Scattering

Mie scattering is a type of scattering of electromagnetic radiation, such as light, by particles of a size comparable to or larger than the wavelength of the radiation. The intensity and pattern of Mie scattering can be affected by the concentration of the scattering particles.

At low concentrations, Mie scattering is typically linearly proportional to the concentration of the scattering particles. This means that if the concentration of the scattering particles is doubled, the intensity of the scattered light will also double. However, at high concentrations, the relationship between Mie scattering and particle concentration becomes more complex.

At high concentrations, the particles can interact with each other, leading to a phenomenon known as multiple scattering. Multiple scattering can cause the scattered light to be redirected and interfered with, resulting in a more complex scattering pattern. In extreme cases, the multiple scattering can lead to a phenomenon known as optical turbidity, where the scattered light is so intense that it can obscure the light source and reduce the visibility of the scattering particles.

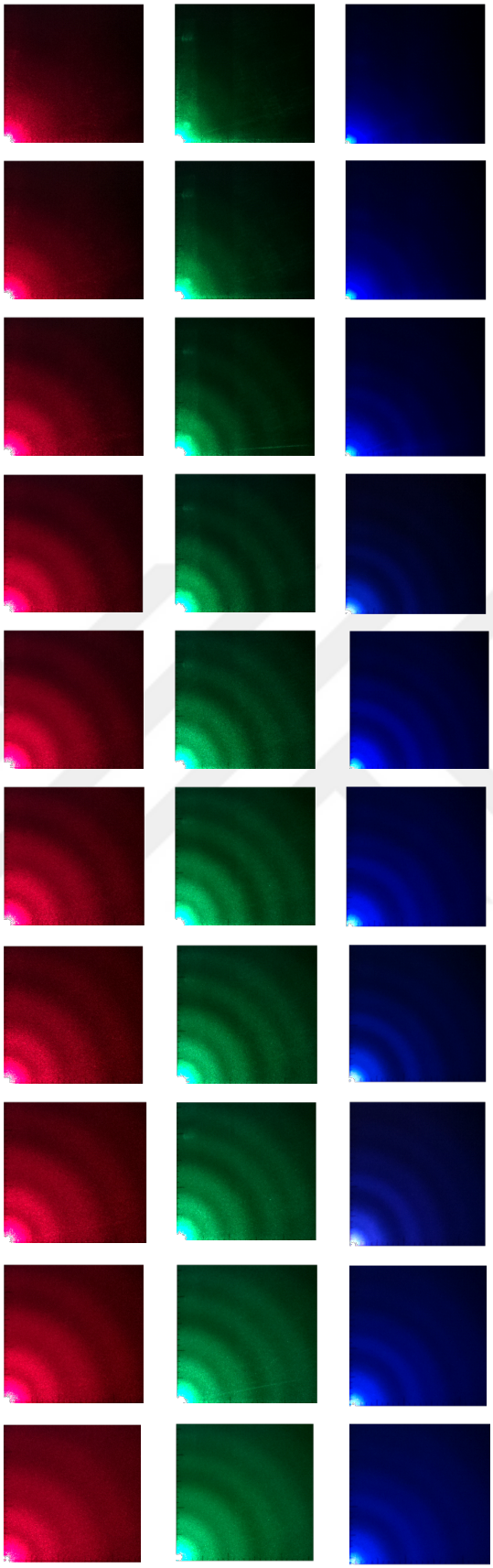

Figure 4.1 Scattering images of Me8 particles by red, green, and blue lasers with increasing concentration.

In summary, the effects of concentration on Mie scattering can range from a linear increase in scattering intensity at low concentrations to complex multiple scattering and optical turbidity at high concentrations.

It was explained in Chapter 1 that forward scattering is dominant in Mie scattering. Considering the equations in the same chapter, when number of the particles increases, the scattered light at close to zero angles, join to the zero-degree scattering, forward scattering, and makes the intensity higher. Therefore, it is expected that increasing the concentration results in more shiny and wider centers on images.

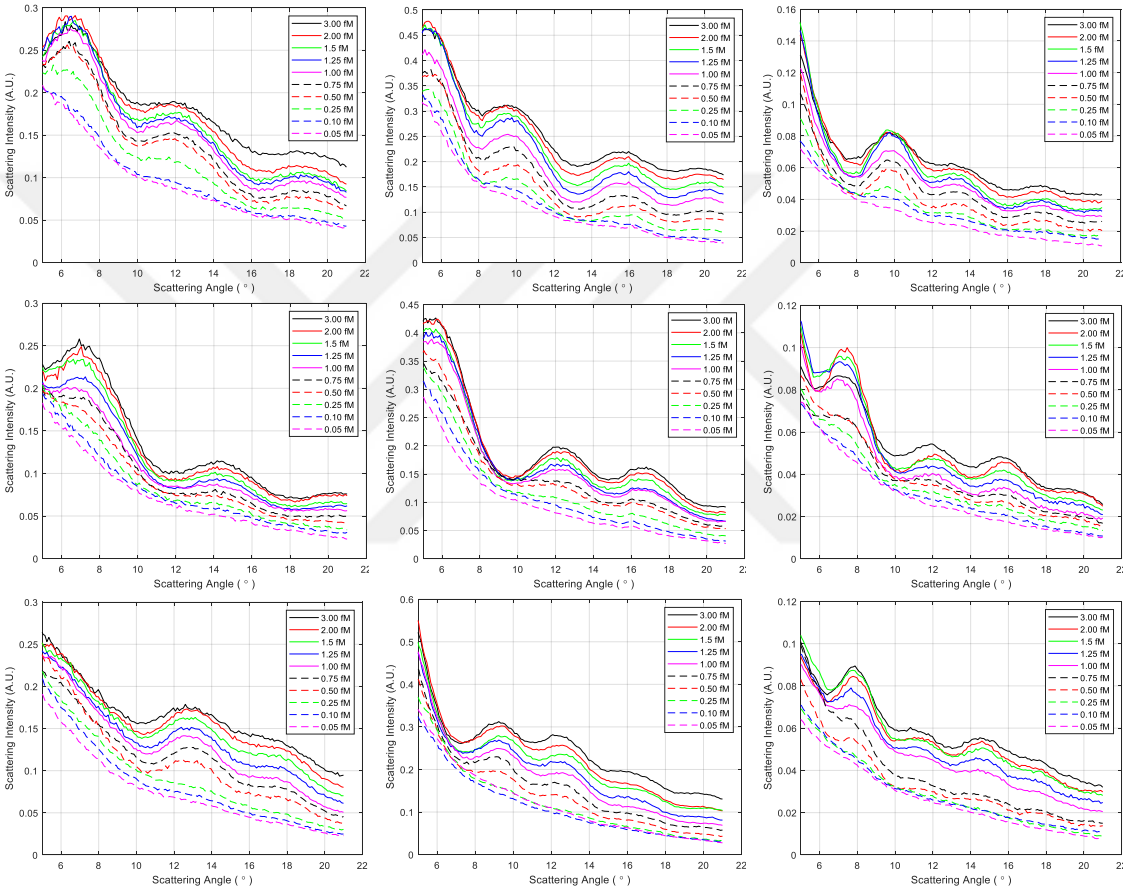

Figure 4.2 Scattering intensity vs concentration change for Me8, PS8 and PS10 materials by red, green, and blue lasers.

In addition to the concentration, the settlement of the particles is also important. As discussed in previous chapters, particles are shaken by vortex before experiments and by hand just before the measurements. However, during the photoshoot, particles move through the bottom of the cuvettes due to gravity. If those particles go down fast, there will be less than targeted concentration and this would lead to less scattering intensity. Less scattering intensity may have two meanings, first, particles move down too fast, and we lose information, second, concentration of the sample is less than targeted. To investigate this issue, instead of 200 images per sample, 800 images were taken

consecutively. Grouping them as 100-image packages and platting their scattering information on the same graph with closest higher and closest lower concentration samples would give us information about reliability of our measurement. In Fig. 4.3, gray-scale images belonging to average of consecutive 100 images of same sample, it was not possible to comment by eye so that we did our image processing steps and obtained scattering lines for those image packages.

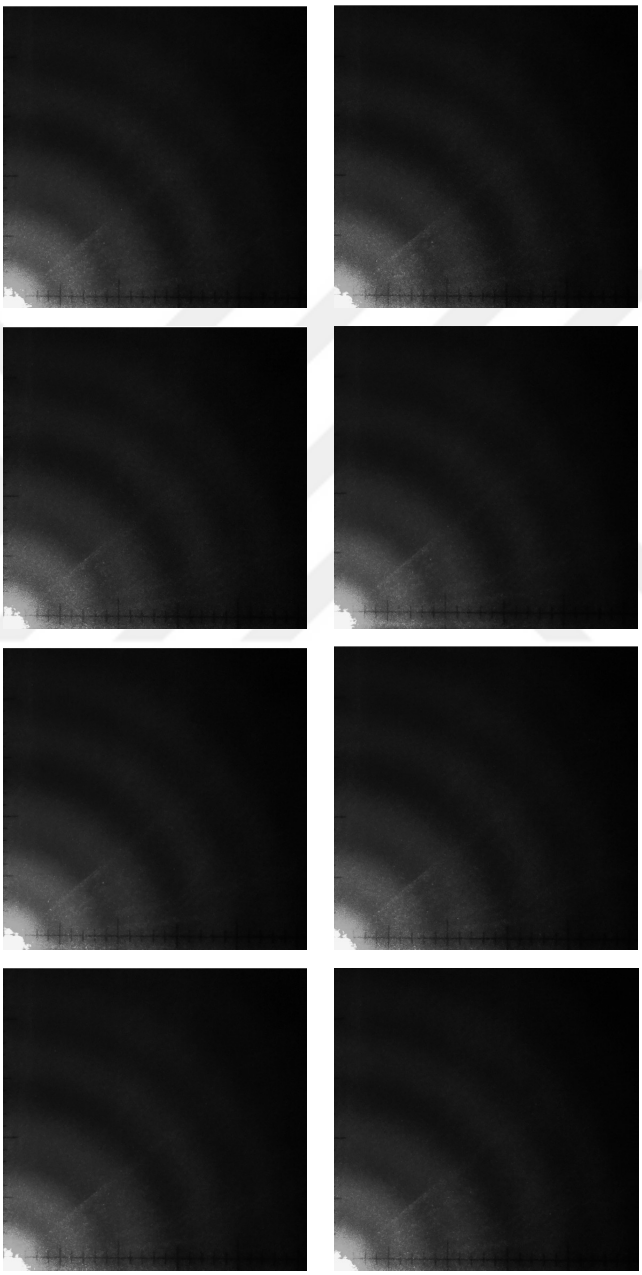

Figure 4.3 Scattering patterns for 2.00 fM PS8 particles for consecutive 100 images.

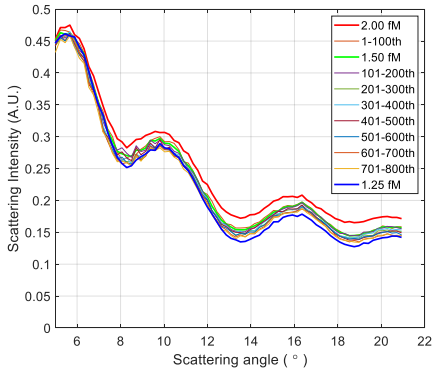

Figure 4.4 Scattering intensity vs time for PS8 particles excited by green laser.

As given in Fig. 4.4, even the last package of 100-image (701-800), meaning that the lowest scattering intensity among the groups, has higher scattering intensity than the closest lower one, 1.25 fM Therefore, we can say that settlement is not an issue on our measurements.

Scattering intensity is important while determining the concentration of particles. The area under scattering lines gives information about how much light scattered and this is directly related to the concentration. We calculated the areas under scattering lines for three different measurements and plotted that data. Then, fitting a curve, calibration curve, provided information about how much amount of scattered light scattered vs concentration. After that point, it is just an image processing step to calculate the value for an unknown concentration to define its value.

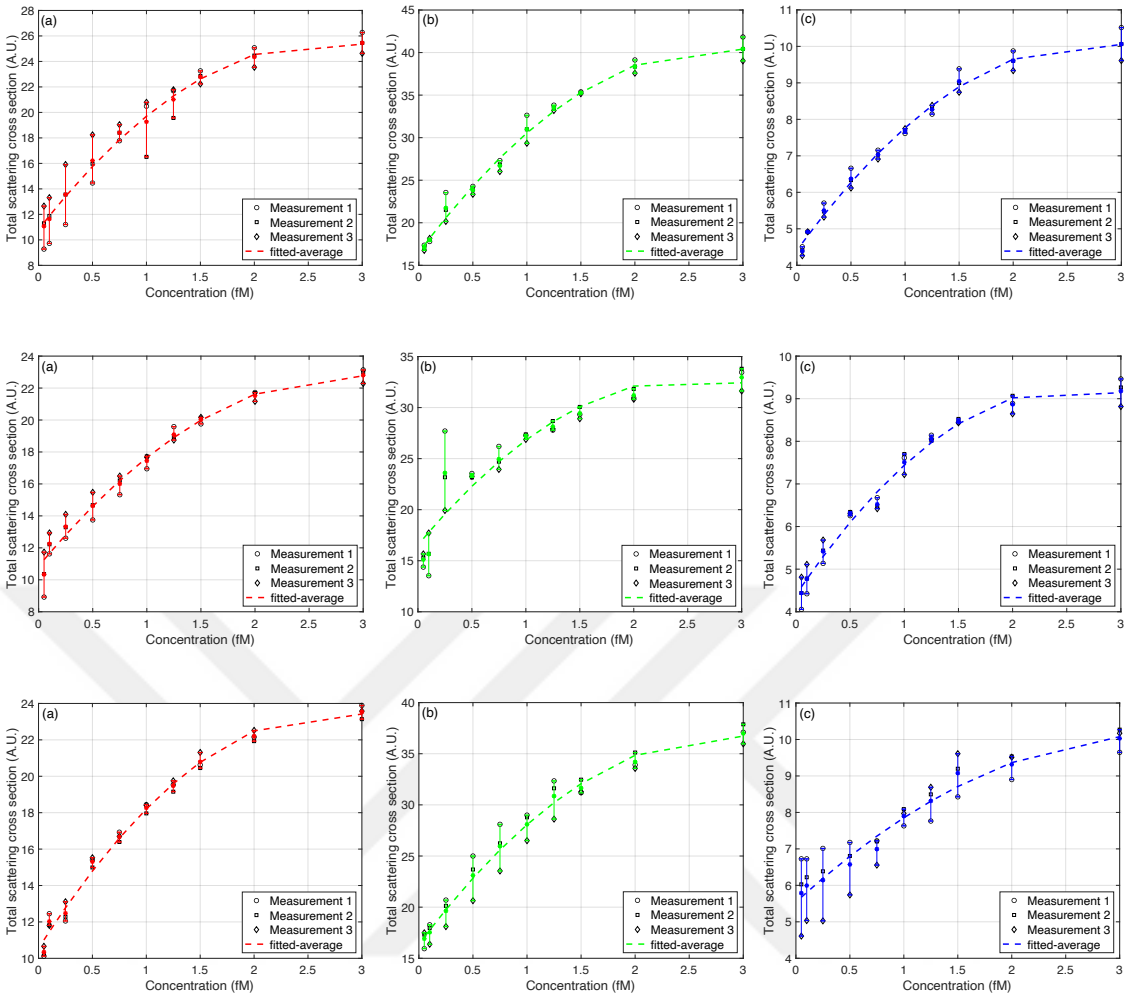

Figure 4.5 Total scattering intensity vs concentration change for Me8, PS8 and PS10 materials by red, green, and blue lasers.

As presented in Fig. 4.5, there are different calibration curves for different particle size, incident wavelength and refractive index. It is known that scattering is dependent on all those parameters. If there is enough number of different particles and lasers, a general equation depending on particle size, refractive index, concentration, power, and wavelength of incident light can be generated.

To sum up, after the experiments, we observed that, as expected, forward scattering gets dominant with increasing concentration. In addition, the same sample scatters at same peak angles, interference rings, and this provides opportunity to use those interference ring angles specifically for that material identification. In our concentration range, because the lines go saturation, it shows that we already reached the limit of our setup to determine the concentration of the samples.

4.2 Effect of Particle Size on Scattering

Mie scattering is a type of scattering phenomenon that occurs when light interacts with particles that are comparable in size to the wavelength of the incident light. In Mie scattering, the scattered light depends strongly on the particle size and the refractive index of the particle.

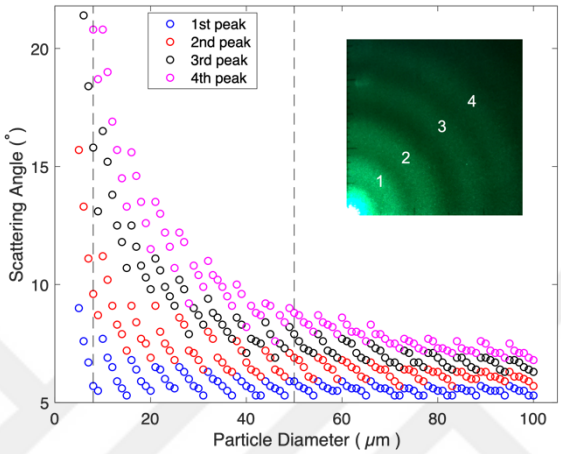

Figure 4.6 Angular distribution of the first four scattering intensity peaks to the particle size as calculated using Mie theory. The particle size was varied between 5-100 µm in water and 514.9 nm incident light beam in MATLAB, (inset) experimental image showing peaks (greater than 5°) for 8 µm.

The size of the particle determines the angle and intensity of the scattered light. In general, smaller particles scatter light more in the forward direction, while larger particles scatter light more in the backward direction. This is because larger particles diffract light more, causing it to scatter in multiple directions.

For a given wavelength of light, there is a characteristic size of particle that scatters the most light in the forward direction, which is called the Mie scattering peak. The Mie scattering peak is shifted to smaller sizes for shorter wavelengths of light.

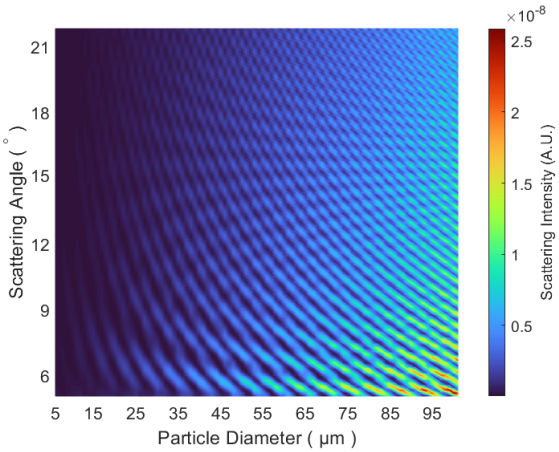

Figure 4.7 Total scattering intensity vs concentration change for Me8, PS8 and PS10 materials by red, green, and blue lasers.

In laboratory experiments, to be able to monitor the effect of particle size, PS8 and PS10 particles were used. 8 and 10 μm size of those particles provided information about particle size parameter when other parameters, i.e., incident wavelength, particle refractive index and concentration, were constant. As expected, when size of Polystyrene particles was increased, forward scattering got dominant. Having more peaks at the same range of scattering angle (5- 21 degree), presents that the scattered light at small angles, got closer even combined with zero-degree scattering. Thus, as given in Fig. 4.7, 10 μm-size PS particles have shiny spot at the center and more bright interference ring at the same range of images.

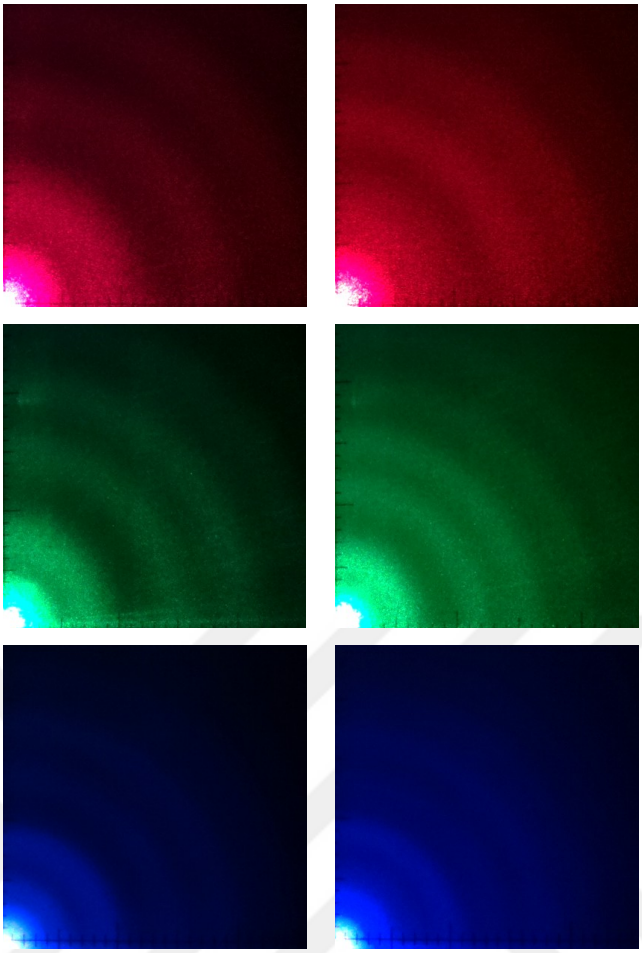

Figure 4.8 Scattering patterns of PS8 and PS10 particles at 1.50 fM concentration to monitor particle size effect by 656.3 nm, 514.9 nm, and 403.8 nm lasers.

In summary, the particle size has a significant effect on Mie scattering, with smaller particles scattering more light in the forward direction, while larger particles scatter more light in the backward direction. The Mie scattering peak is shifted to smaller sizes for shorter wavelengths of light.

4.3 Effect of Particle Refractive Index on Scattering

In Mie scattering, the refractive index of particles plays an important role in determining the scattering pattern. Mie scattering is a type of elastic scattering of light by spherical particles, where the size of the particle is on the same order as the wavelength of light. The refractive index of a material is a measure of the speed of light in that material and how it bends when it passes through the material.

The refractive index of particles affects the scattering pattern because it determines the phase shift of the scattered wave relative to the incident wave. This phase shift is

caused by the change in the speed of light as it passes from one medium (air) to another (the particle).

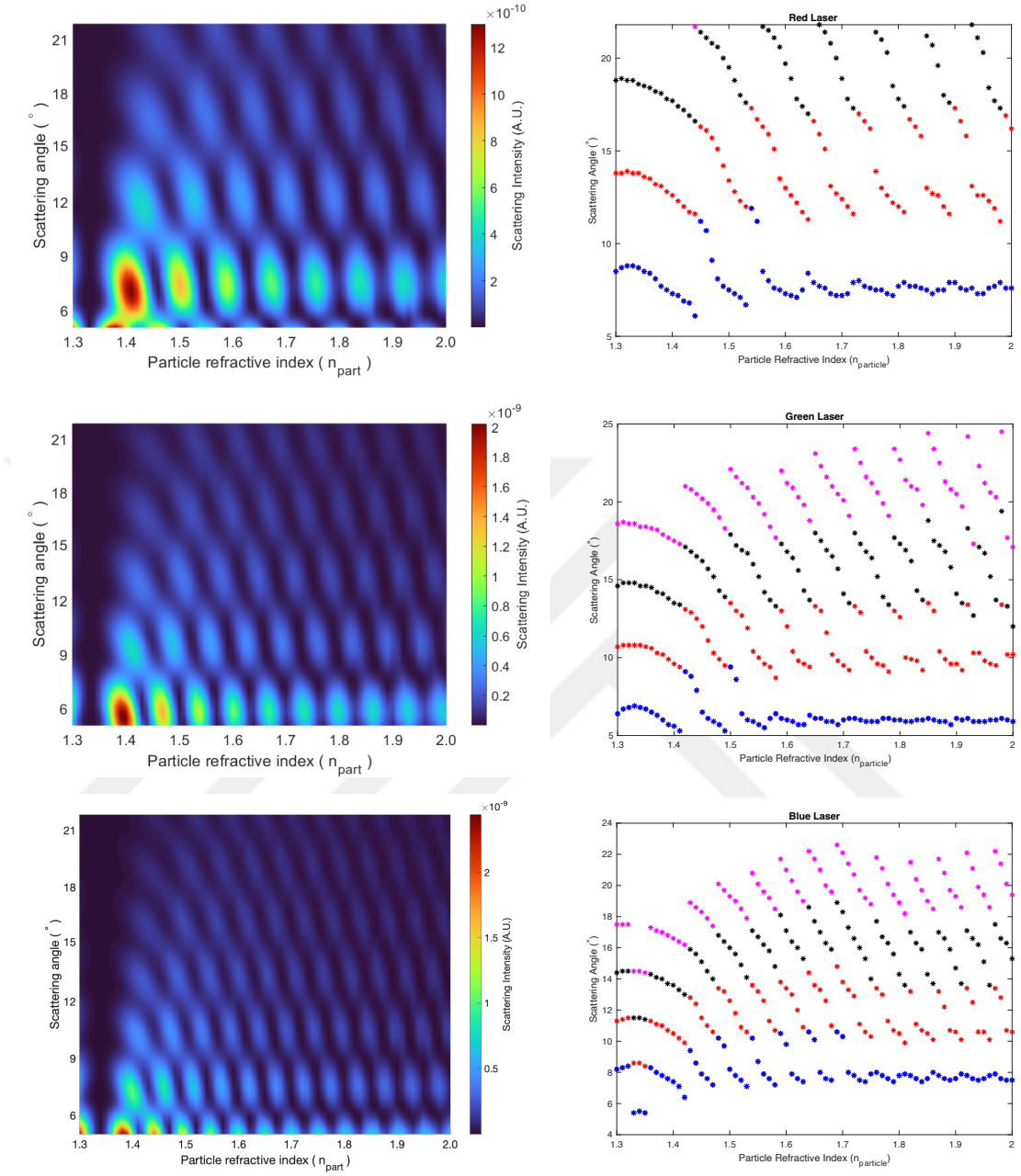

Figure 4.9 Scattering intensities vs particle refractive index for red, green, and blue lasers, respectively (left column), locations of first four peak angles vs particle refractive index for reg, green, and blue lasers, respectively (right column)

In particular, the refractive index affects the scattering angle at which the scattered light is most intense. The angle is known as the "scattering angle." As the refractive index of the particle increases, the scattering angle decreases. Additionally, the refractive index affects the polarization of the scattered light.

In laboratory, Me8 and PS8 particles were used to investigate the effect of particle refractive index. This is one of the key points of this study because -it is worth to say

again- there is lack of study in terms of same size and shape but material of particle in the literature. In theory, if a particle has higher refractive index value compared to the particles having lower refractive index, it scatters the light with wider angles. Therefore, at the same range of distance from the center on an image, a smaller number of bright interference rings are observed. As presented in Fig. 4.9, left column (Me8 with lower refractive index) has more rings compared to the right one (PS8 with higher refractive index). It shouldn't be forgotten to compare the refractive indices at proper wavelengths due to dispersion.

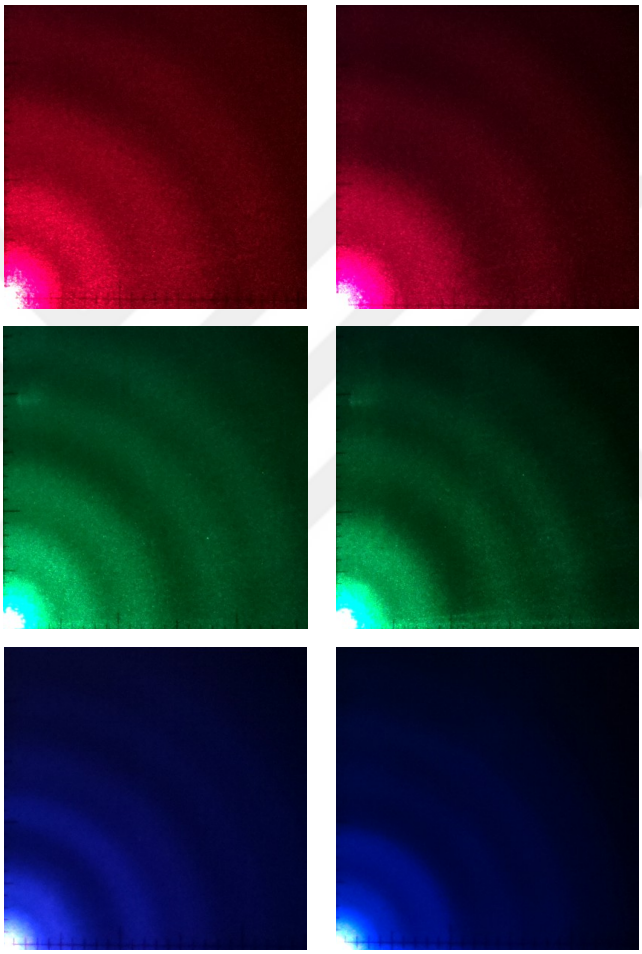

Figure 4.10 Scattering patterns of Me8 and PS8 particles at 1.50 fM concentration to monitor refractive index effect by 656.3 nm, 514.9 nm, and 403.8 nm lasers.

In summary, the refractive index of particles plays a crucial role in Mie scattering by influencing the scattering angle and polarization of the scattered light.

4.4 Effect of Incident Wavelength on Scattering

Mie scattering is a type of elastic scattering that occurs when a beam of electromagnetic radiation interacts with particles that are larger than the wavelength of the incident radiation. In Mie scattering, the scattered radiation is dependent on the size, shape, and refractive index of the particles as well as the incident wavelength of the radiation.

The size parameter, which is defined as the ratio of the particle radius to the incident wavelength, determines the scattering behavior of Mie scattering. As the size parameter increases, the scattering pattern changes from forward scattering to backward scattering.

In general, for small particles (size parameter << 1), the scattering is strongly dependent on the incident wavelength.

Mie scattering is a type of scattering phenomenon that occurs when electromagnetic radiation, such as light, interacts with spherical particles that are similar in size to the wavelength of the incident radiation. The size of the particles and the wavelength of the incident radiation play a crucial role in determining the characteristics of Mie scattering.

The incident wavelength has a significant effect on Mie scattering. When the size of the spherical particle is comparable to the wavelength of the incident radiation, the scattered light undergoes constructive and destructive interference, leading to complex scattering patterns. This phenomenon is known as resonance scattering. The resonance wavelength, at which the scattering is the strongest, depends on the size and refractive index of the particle.

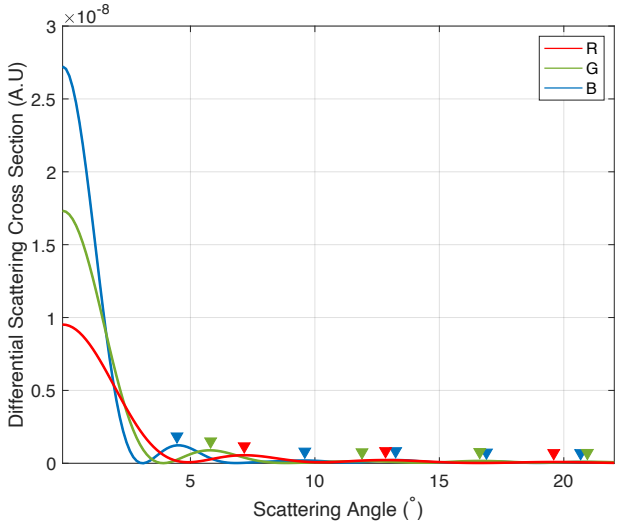

Figure 4.11 Calculated angular distribution of the scattering cross-section of 8 µm-sized particle in water for three different incident wavelengths. The triangles represent the locations of the scattering peaks.

As the incident wavelength increases, the scattering becomes less sensitive to the size of the particle, and the scattering pattern becomes more uniform. This is because the effect of resonance scattering diminishes as the size of the particle becomes small compared to the wavelength of the incident radiation. In this case, the scattering pattern becomes more similar to Rayleigh scattering, which occurs when the size of the particle is much smaller than the wavelength of the incident radiation.

It is starting point of this study in the laboratory. We were expecting that different incident wavelengths (lasers) needed to provide different patterns of scattering and it had to be observable. In addition, different sizes of same particle and different particles at same size were aimed to be resulted in different images. All those expectations occurred successfully. Using a cost-effective setup, a few hundreds of euros, we were able to observe those different patterns clearly. In addition, three different sample sets and measurements at different times provided consistent results.

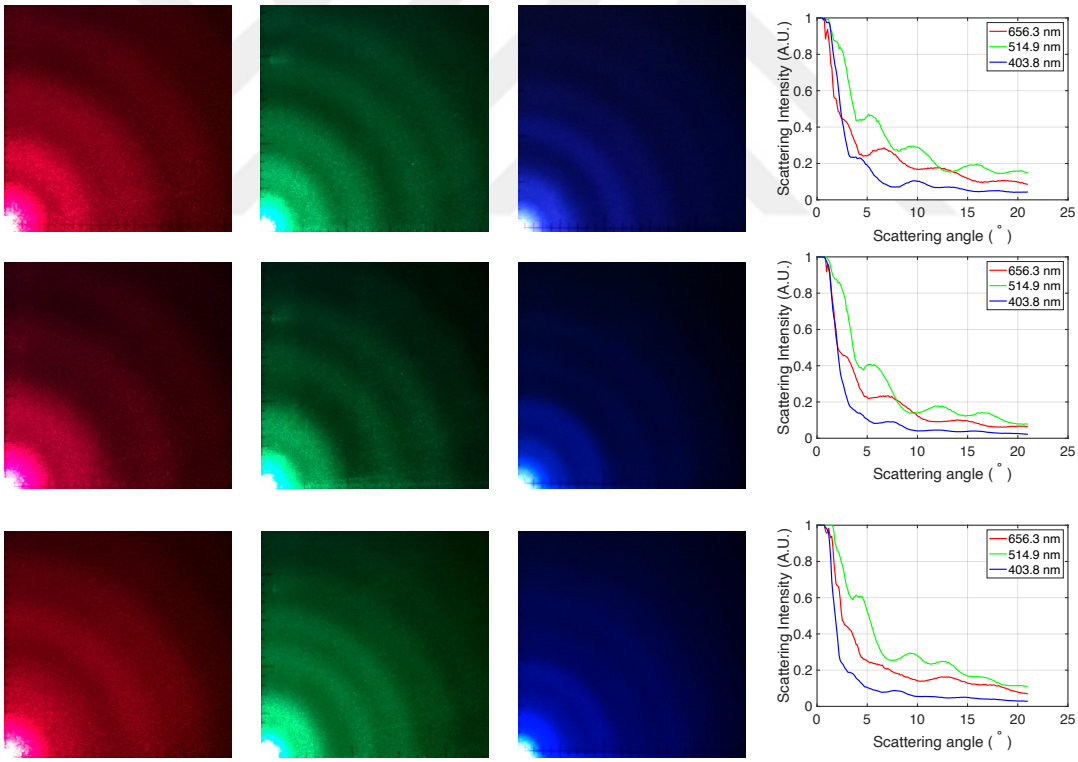

Figure 4.12 Scattering patterns of Me8, PS8, and PS10 particles at 1.50 fM concentration and their scattering data to monitor incident wavelength effect by 656.3 nm, 514.9 nm, and 403.8 nm lasers.

In summary, the incident wavelength affects Mie scattering by determining the resonance wavelength, which is the wavelength at which scattering is the strongest. As

the wavelength increases, the scattering becomes less sensitive to the size of the particle and the scattering pattern becomes more uniform.

Chapter 5

Machine Learning Integration

In previous chapters, it was showed that the equations to calculate scattering is difficult and complex for hand-calculations. Thus, they were embedded to numerical solvers. However, for rapid analysis and ease of use, integration of machine learning to the setup would create a dramatical increase on the performance of this study.

Using the equations, peak angles (bright interference ring angles) are obtained from the theory. In real life application, instead of the inputs which we use to get those peak angles, we have the output, the pattern of scattering .So, reverse engineering is needed on the theoretical calculations. In this study, we aimed to show the match between theory and experimental results which are limited by two materials, Me and PS. Furthermore, only 8 and 10 μm-sized particles were used to prepare samples for investigation. There will be much more options in real life applications.

In Fig. 5.1, it is presented that the match between theory and experimental results are satisfying. Small differences between those two types of results, provided opportunity to create a dataset for further developments.

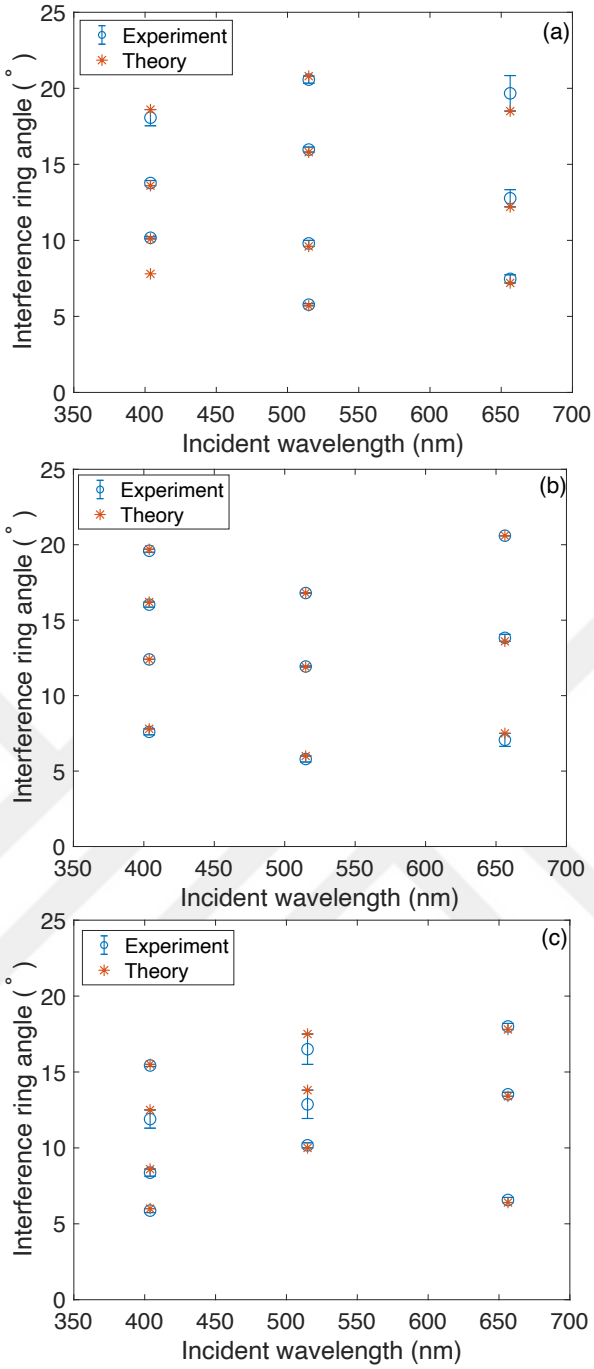

Figure 5.1 Differences between Me8, PS8 and P10 particles at 1.50 fM concentration to monitor consistency between experiments and theory by 656.3 nm, 514.9 nm, and 403.8 nm lasers.

To check consistency of experimental results, at different times (at least 3 months period), we prepared sample sets and got images of scattering. Once those experiments completed, we calculated standard deviations between those experiments, and got their average to decrease experimental error and to use as the final experimental results Then, mean absolute percentage error and root mean square errors were calculated between the

theory (MATLAB) and experimental results, as showed in Table 5.1. Statistical t-tests showed that there is no meaningful difference between those data.

Table 5.1 Matching of experimental and three experimental peak angles (P1, P2, P3, P4) with standard deviation and error calculations for red (R), green (G), and blue (B) lasers.

		Theory			Experiment (170 µW)			Experiment (150 µW)			Experiment (160 µW)		
		R	**G**	**B**	**R**	**G**	**B**	**R**	**G**	**B**	**R**	**G**	**B**
Me8	**P1**	7,2	5,7	7,8	7,6	5,9	NA	7,4	5,7	NA	7,4	5,7	NA
	P2	12,2	9,6	10,1	12,8	9,8	10,2	12,7	9,7	10,1	12,8	9,9	10,2
	P3	18,5	15,8	13,6	19,7	16,0	13,6	19,5	15,9	14,0	19,8	16,0	13,7
	P4	NA	20,8	18,6	NA	20,6	18,2	NA	20,6	17,9	NA	20,5	18,1
PS8	**P1**	7,5	6,0	7,8	6,7	5,8	7,5	7,2	5,7	7,6	7,3	5,9	7,7
	P2	13,6	11,9	12,4	13,9	12,1	12,2	14,0	11,9	12,5	13,6	11,8	12,5
	P3	20,6	16,8	16,2	20,7	16,9	16,0	20,6	16,7	16,1	20,5	16,8	16,0
	P4	NA	NA	19,7	NA	NA	19,6	NA	NA	19,7	NA	NA	19,5
PS10	**P1**	6,4	10,0	6,0	6,6	10,2	6,0	6,6	10,1	5,7	6,5	10,2	5,9
	P2	13,4	13,8	8,6	13,5	12,5	8,3	13,6	12,9	8,4	13,5	13,2	8,4
	P3	17,8	17,5	12,5	17,9	16,3	11,8	18,1	16,6	11,9	18,0	16,6	12,0
	P4	NA	NA	15,5	NA	NA	15,6	NA	NA	15,4	NA	NA	15,3
		STD			**AVEG**			**MAPE**			**RMSE**		
		R	**G**	**B**	**R**	**G**	**B**	**R**	**G**	**B**	**R**	**G**	**B**
Me8	**P1**	0,12	0,12	NA	7,47	5,77	NA	3,70	1,17	NA	0,28	0,12	NA
	P2	0,06	0,10	0,06	12,77	9,80	10,17	4,64	2,08	0,66	0,57	0,22	0,08
	P3	0,15	0,06	0,21	19,67	15,97	13,77	6,31	1,05	1,23	1,17	0,17	0,24
	P4	NA	0,06	0,15	NA	20,57	18,07	NA	1,12	2,87	NA	0,24	0,55
PS8	**P1**	0,32	0,10	0,10	7,07	5,80	7,60	5,78	3,33	2,56	0,51	0,22	0,22
	P2	0,21	0,15	0,17	13,83	11,93	12,40	1,72	0,28	0,00	0,29	0,13	0,14
	P3	0,10	0,10	0,06	20,60	16,80	16,03	0,00	0,00	1,03	0,08	0,08	0,17
	P4	NA	NA	0,10	NA	NA	19,60	NA	NA	0,51	NA	NA	0,13
PS10	**P1**	0,06	0,06	0,15	6,57	10,17	5,87	2,60	1,67	2,22	0,17	0,17	0,18
	P2	0,06	0,35	0,06	13,53	12,87	8,37	1,00	6,76	2,71	0,14	0,98	0,24
	P3	0,10	0,17	0,10	18,00	16,50	11,90	1,12	5,71	4,80	0,22	1,01	0,61
	P4	NA	NA	0,15	NA	NA	15,43	NA	NA	0,43	NA	NA	0,14

5.1 Dataset Creation

After showing the appropriate match between the lab results and theoretical calculations, we created a dataset on MATLAB, and the code for it is given in Appendix B. Using nested for loops of scattering parameters, i.e., particle size, refractive index of the particles and medium, incident wavelength, a dataset was created on MATLAB. Considering the limitations of the setup and the literature, we defined appropriate ranges for particle size and refractive indices. For incident wavelength, we used the same ones, 656.3 nm, 514.9 nm, and 403.8 nm, with the ones we have in the laboratory. Starting from 5 μm to 13 μm with 0.5 μm increments for particle diameter, and from 1.3 to 2.2 with 0.01 increments of refractive index were the ranges of this nested for loop operation. In total 4641lines were obtained including peak angle values (P1, P2, P3, P4) for each combination of for loop parameters. A few lines from the dataset are presented in Table 5.2.

Table 5.2 A few sample lines of the dataset created on MATLAB to be used in Random Forest Algorithm.

Inc. Wl. (nm)	Particle Size	Particle Ref. Index	Medium Ref. Index	P1	P2	P3	P4
403,8	5	2,18	1,3388	7,4	12,6	21,4	0,0
403,8	5	2,19	1,3388	7,4	12,4	21,0	0,0
403,8	5	2,20	1,3388	7,2	12,0	19,7	0,0
403,8	5,5	1,30	1,3388	7,4	12,2	16,7	21,4
403,8	5,5	1,31	1,3388	7,5	12,2	16,8	21,4
403,8	5,5	1,32	1,3388	7,8	12,4	16,8	21,4

Then, we trained two different models, Model 1 for particle size, and Model 2 for particle refractive index. We used randomly selected 80% of this main dataset after adjustments to give it as training data to the model. 20 iterations with 100 trees were used in model, as commonly done in literature [35]. Once the training had been completed, the remain part, 20%, was used to test the performance of the model. It is worth to say that, until this step, it was all done using the data created on MATLAB by theoretical calculations.

5.2 Model-1 Particle Size

Modifications were needed on the dataset for each model. For Model 1, particle size estimation, refractive index data were not given as input. Only incident wavelength,

refractive index of the medium (in consistency with incident light) and first four peak angles were used as the input. So, 6 numbers were the input for a line from dataset and as seventh, particle size was added, as presented in Appendix C.

After 20 iterations and calculation of accuracy for each iteration, the average accuracy was calculated for the final accuracy of the model with test data from main dataset.

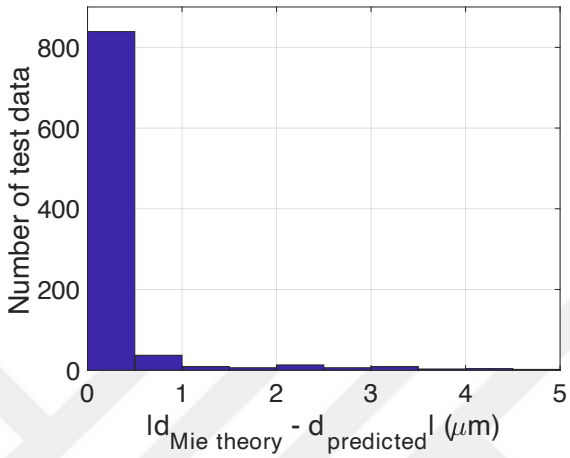

Figure 5.2 Histogram of the differences between real and estimated particle size for randomly selected 20% of the dataset.

As presented in Fig. 5.2, most of the test results have an error less than 0.5 μm compared to real values. The correlation between real and estimated results is 0.95. Thus, we are able to say that we trained a successful model to predict particle size from incident wavelength, refractive index of the medium and first four bright interference rings of scattering.

Although obtaining promising results by test data created on MATLAB, the important point is having the same performance from experimental results as test data. Prediction of particle size will be meaningful if the model could determine it successfully. Therefore, we used laboratory results as new test data for the Model 1. As given in Table 5.3, among 9 test data, 3 particles by three incident light, the highest error is 1.5 μm which is for PS8 by red light. Other than that, we only have 0.5 μm difference between theory and prediction. T-tests also showed that there is no significant difference between those two types of data, theory, and prediction.

Table 5.3 Real and predicted values of particles sizes for experimental results as test data for Model 1.

	Red (656.3 nm)			Green (514.9 nm)			Blue (403.8 nm)		
	Me8	**PS8**	**PS10**	**Me8**	**PS8**	**PS10**	**Me8**	**PS8**	**PS10**
Real	8 μm	8 μm	10 μm	8 μm	8 μm	10 μm	8 μm	8 μm	10 μm
Predicted	8 μm	6.5 μm	10 μm	8 μm	8 μm	10 μm	8 μm	8 μm	9.5 μm

In summary, our random forest algorithm integrated setup was able to define particle size. We proved that it is possible to do classifications, estimations with a cost-effective, simple, and portable device.

5.3 Model-2 Particle Refractive Index

As modifications on main dataset for Model 2, particle refractive index estimation, particle size data were not given as input. Only incident wavelength, refractive index of the medium (in consistency with incident light) and first four peak angles were used as the input. So, 6 numbers were the input for a line from dataset and as seventh, particle refractive index was added, as presented in Appendix D.

After 20 iterations and calculation of accuracy for each iteration, the average accuracy was calculated for the final accuracy of the model with test data from main dataset.

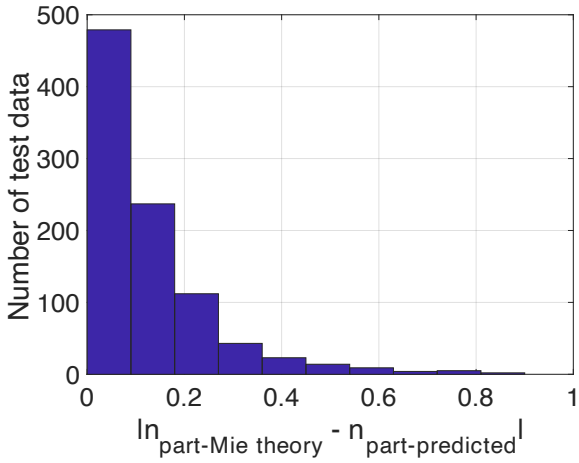

Figure 5.3 Histogram of the differences between real and estimated particle refractive index for randomly selected 20% of the dataset.

As presented in Fig. 5.3, most of the test results have an error less than 0.5 compared to real values. The correlation between real and estimated results is 0.748. Thus, we are able to say that we trained a successful model to predict particle refractive index from incident wavelength, refractive index of the medium and first four bright interference rings of scattering.

Although obtaining promising results by test data created on MATLAB, the important point is having the same performance from experimental results as test data. Prediction of particle refractive index will be meaningful if the model could determine it successfully. In addition, this is one of the key points of this study, considering the estimation of refractive indices of same-sized spheres. Therefore, we used laboratory results as new test data for the Model 2. As given in Table 5.4, among 9 test data, 3 particles by three incident light, the highest error is about 0.13 which is for PS8 by red light. Other than that, it is clearly can be seen that Me8 parameters were estimated identically. PS10 has better prediction than PS8. T-tests also showed that there is no significant difference between those two types of data, theory, and prediction.

Table 5.4 Real and predicted values of particles refractive indices of Me8, PS8, and PS10 by 403.8 nm, 514.9 nm, and 656.3 nm lasers.

	Red (656.3 nm)			**Green (514.9 nm)**			**Blue (403.8 nm)**		
	Me8	**PS8**	**PS10**	**Me8**	**PS8**	**PS10**	**Me8**	**PS8**	**PS10**
Real	1.79	1.589	1.589	1.89	1.601	1.601	1.96	1.617	1.617
Predicted	1.79	1.72	1.61	1.89	1.60	1.60	1.96	1.56	1.66

Chapter 6

Conclusions and Future Prospects

6.1 Conclusions

There will be conclusions in this part.

6.2 Societal Impact and Contribution to Global Sustainability

The societal impact of microplastics is significant. The increasing amount of microplastics in our environment has raised public awareness of the plastic pollution problem and has led to calls for action from consumers, businesses, and governments. People are becoming more conscious of their plastic use and are actively seeking out alternative solutions. Furthermore, companies are also changing their practices and developing sustainable packaging alternatives. However, the problem of microplastics requires a global effort to mitigate its impact.

The issue of microplastics is closely linked to the United Nations' Sustainable Development Goals (SDGs). SDG 14, Life Below Water, specifically aims to conserve and sustainably use the oceans, seas, and marine resources for sustainable development. Microplastics have been identified as a major threat to marine ecosystems, and addressing the issue is crucial in achieving SDG 14.

Furthermore, microplastics also have implications for other SDGs. For example, SDG 12, Responsible Consumption and Production, emphasizes the need for sustainable consumption and production patterns to minimize waste generation and reduce the negative impacts of consumption on the environment. Addressing microplastics requires a shift towards sustainable consumption and production patterns that prioritize reducing plastic use and promoting proper waste management practices.

Moreover, microplastics can have implications for human health, which is addressed by SDG 3, Good Health, and Well-being. It is important to address the issue of microplastics to protect both marine and human health.

In conclusion, addressing the issue of microplastics is crucial in achieving multiple SDGs. It requires a global effort to reduce plastic use, promote sustainable consumption and production patterns, and develop effective waste management systems. By addressing the issue of microplastics, we can promote a more sustainable and healthy future for our planet and its inhabitants.

It is important for governments and organizations to work together to address this issue and develop policies and initiatives to reduce plastic use and improve waste management systems. By working together, we can create a more sustainable future for our planet.

6.3 Future Prospects

In terms of this study, the setup can be used for different type of samples, i.e., DNAs, bacteria, cells, metallic particles etc. To investigate nano-size particles, a thin lens may be needed to focus light on a much smaller area. In addition, by using appropriate solvents, solid samples can be diluted and examined after some filtering and basic preprocessing steps.

In general, the issue of microplastics is expected to continue to be a major concern in the future, as plastic production and consumption continue to increase globally. However, there are also promising prospects for addressing the issue and detecting microplastics in the environment.

In terms of addressing the issue, there is growing awareness among consumers, businesses, and governments about the negative impacts of microplastics on the environment and human health. This has led to a push for reducing plastic use and improving waste management systems. Additionally, there is ongoing research into sustainable alternatives to plastic and innovative technologies for capturing and removing microplastics from the environment.

In terms of detection, there have been advancements in analytical methods for identifying and quantifying microplastics in different environmental samples. These include techniques such as Raman spectroscopy, Fourier-transform infrared

spectroscopy, and pyrolysis-gas chromatography-mass spectrometry. Furthermore, there is ongoing research into developing more efficient and cost-effective methods for detecting microplastics, such as biosensors and microfluidic devices.

Overall, the future prospects of the microplastics issue and detection are both challenging and promising. Addressing the issue will require a concerted effort from individuals, businesses, and governments to reduce plastic use, improve waste management systems, and invest in sustainable alternatives. At the same time, ongoing research into detection technologies will be crucial in identifying the extent of the problem and developing effective mitigation strategies.

BIBLIOGRAPHY

[1] E. J. Carpenter and K. L. Smith, “Plastics on the Sargasso Sea Surface,” *Science (1979)* **175**, 1240–1241 (1972).

[2] E. J. Carpenter, S. J. Anderson, G. R. Harvey, H. P. Miklas, and B. B. Peck, “Polystyrene Spherules in Coastal Waters,” *Science (1979)* **178**, 749–750 (1972).

[3] A. Ashkin, “Acceleration and Trapping of Particles by Radiation Pressure,” *Phys Rev Lett* **24**, 156 (1970).

[4] J. A. Ivar Do Sul and M. F. Costa, “The present and future of microplastic pollution in the marine environment,” *Environmental Pollution* **185**, 352–364 (2014).

[5] S. L. Wright, R. C. Thompson, and T. S. Galloway, “The physical impacts of microplastics on marine organisms: a review.,” *Environ Pollut* **178**, 483–492 (2013).

[6] B. E. Oßmann, G. Sarau, H. Holtmannspötter, M. Pischetsrieder, S. H. Christiansen, and W. Dicke, “Small-sized microplastics and pigmented particles in bottled mineral water,” *Water Res* **141**, 307–316 (2018).

[7] A. Dick Vethaak and J. Legler, “Microplastics and human health,” *Science (1979)* **371**, 672–674 (2021).

[8] K. D. Cox, G. A. Covernton, H. L. Davies, J. F. Dower, F. Juanes, and S. E. Dudas, “Human Consumption of Microplastics,” *Environ Sci Technol* **53**, 7068–7074 (2019).

[9] D. Schymanski, C. Goldbeck, H. U. Humpf, and P. Fürst, “Analysis of microplastics in water by micro-Raman spectroscopy: Release of plastic particles from different packaging into mineral water,” *Water Res* **129**, 154–162 (2018).

[10] Richard Kirby, “The Nitty Gritty on Microplastics,” <https://whalewatchingauckland.com/blog/the-nitty-gritty-on-microplastics/> (29 April 2023).

[11] Per Harald Olsen, “Water flea (Daphnia magna Straus),” *NTNU - Norges teknisk-naturvitenskapelige universitet*, <https://www.artsdatabanken.no/Taxon/Daphnia%20magna/123935> (29 April 2023).

[12] A. Isobe, S. Iwasaki, K. Uchida, and T. Tokai, “Abundance of non-conservative microplastics in the upper ocean from 1957 to 2066,” *Nature Communications 2019 10:1* **10**, 1–13 (2019).

[13] K. E. Peiponen, J. Räty, U. Ishaq, S. Pélisset, and R. Ali, “Outlook on optical identification of micro- and nanoplastics in aquatic environments,” *Chemosphere* **214**, 424–429 (2019).

[14] M. F. Costa, J. A. Ivar Do Sul, J. S. Silva-Cavalcanti, M. C. B. Araújo, Â. Spengler, and P. S. Tourinho, "On the importance of size of plastic fragments and pellets on the strandline: A snapshot of a Brazilian beach," *Environ Monit Assess* **168**, 299–304 (2010).

[15] A. Tahir, M. F. Samawi, K. Sari, R. Hidayat, R. Nimzet, E. A. Wicaksono, L. Asrul, and S. Werorilangi, "Studies on microplastic contamination in seagrass beds at Spermonde Archipelago of Makassar Strait, Indonesia," *J Phys Conf Ser* **1341**, 022008 (2019).

[16] P. K. Cheung and L. Fok, "Evidence of microbeads from personal care product contaminating the sea," *Mar Pollut Bull* **109**, 582–585 (2016).

[17] S. Sridharan, M. Kumar, L. Singh, N. S. Bolan, and M. Saha, "Microplastics as an emerging source of particulate air pollution: A critical review," *J Hazard Mater* **418**, 126245 (2021).

[18] P. Orellano, J. Reynoso, N. Quaranta, A. Bardach, and A. Ciapponi, "Short-term exposure to particulate matter (PM10 and PM2.5), nitrogen dioxide (NO2), and ozone (O3) and all-cause and cause-specific mortality: Systematic review and meta-analysis," *Environ Int* **142** (2020).

[19] "Microplastics and Their Impacts on Organisms and Trophic Chains," 2022, <https://www.mdpi.com/journal/water/special_issues/Microplastics_Impacts#info> (29 April 2023).

[20] E. A. Shore, J. A. deMayo, and M. H. Pespeni, "Microplastics reduce net population growth and fecal pellet sinking rates for the marine copepod, Acartia tonsa," *Environmental Pollution* **284**, 117379 (2021).

[21] O. Olatunji, "Microplastics: Emerging Issues in Emerging Urbanization," *Plastic and Polymer Industry by Region*, 177–199 (2022).

[22] P. M. Potter, "Microplastics: emerging trends and research gaps," *ACS Spring 2021 National Meeting* (2021).

[23] L. G. A. Barboza, A. Dick Vethaak, B. R. B. O. Lavorante, A. K. Lundebye, and L. Guilhermino, "Marine microplastic debris: An emerging issue for food security, food safety and human health," *Mar Pollut Bull* **133**, 336–348 (2018).

[24] C. Rubio-Armendáriz, S. Alejandro-Vega, S. Paz-Montelongo, Á. J. Gutiérrez-Fernández, C. J. Carrascosa-Iruzubieta, and A. Hardisson-de la Torre, "Microplastics as Emerging Food Contaminants: A Challenge for Food Safety," *Int J Environ Res Public Health* **19** (2022).

[25] S. A. Mason, V. G. Welch, and J. Neratko, "Synthetic Polymer Contamination in Bottled Water," *Front Chem* **6**, 407 (2018).

[26] J. Barrett, Z. Chase, J. Zhang, M. M. B. Holl, K. Willis, A. Williams, B. D. Hardesty, and C. Wilcox, "Microplastic Pollution in Deep-Sea Sediments from the Great Australian Bight," *Front Mar Sci* **7**, 808 (2020).

[27] J. Vieira Dantas Filho, V. Perez Pedroti, B. L. Temponi Santos, M. M. de Lima Pinheiro, Á. Bezerra de Mira, F. Carlos da Silva, E. C. Soares e Silva, J. Cavali, E. A. Cecilia Guedes, et al., "First evidence of microplastics in freshwater from fish farms in Rondônia state, Brazil," *Heliyon* **9**, e15066 (2023).

[28] Blazej Kupec, "What is Microfiber Pollution and How Can We Stop It," 2021, <https://blog.planetcare.org/what-is-microfiber-pollution-and-how-can-we-stop-it/> (29 April 2023).

[29] "Light Scattering ," 2019, <https://physicsopenlab.org/2019/07/10/light-scattering/> (29 April 2023).

[30] A. Karami, A. Golieskardi, C. Keong Choo, V. Larat, T. S. Galloway, and B. Salamatinia, "The presence of microplastics in commercial salts from different countries," *Scientific Reports 2017 7:1* **7**, 1–11 (2017).

[31] B. Balogun and A. Timothy, "PRODUCTION AND CHARACTERIZATION OF MELAMINE-FORMALDEHYDE MOULDING POWDER," *International Journal of Advanced Academic Research | Sciences* **6**, 2488–9849 (2020).

[32] "CRC Handbook of Chemistry and Physics," *CRC Handbook of Chemistry and Physics* (2016).

[33] "Melamine," <https://www.chembk.com/en/chem/Melamine> (29 April 2023).

[34] J. L. Speiser, M. E. Miller, J. Tooze, and E. Ip, "A Comparison of Random Forest Variable Selection Methods for Classification Prediction Modeling," *Expert Syst Appl* **134**, 93–101 (2019).

[35] G. Biau and E. Scornet, "A random forest guided tour," *Test* **25**, 197–227 (2016).

[36] M. Z. Joharestani, C. Cao, X. Ni, B. Bashir, and S. Talebiesfandarani, "PM2.5 Prediction Based on Random Forest, XGBoost, and Deep Learning Using Multisource Remote Sensing Data," *Atmosphere 2019, Vol. 10, Page 373* **10**, 373 (2019).

[37] "Random Trees classifier," <https://catalyst.earth/catalyst-system-files/help/concepts/focus_c/oa_classif_intro_rt.html> (29 April 2023).

APPENDIX A

Code for Scattering

```
d=8e-6;          %sphere diameter
m_sph=1.79;      %sphere refractive index
m_env=1.331;     %medium refractive index
l_vac=656.3e-9;  %wavelength in vacuum

%H20:  1.3310R, 1.3344G, 1.3388B
%ME:   1.79-R, 1.89-G, 1.96-B
%PS:   1.589-R, 1.601-G, 1.617-B


%%%%%%%% CALCULATIONS START AFTER HERE
%%%%%%%%%%%%%%%%%
a=d/2;
k=2*pi/(l_vac/m_env);
x=k*a;%DWH eq.1
m=m_sph/m_env;

M=ceil(x + 4*(x^(1/3) + 2));
n=1:M;

fpsi=sqrt(pi*x/2)*besselj(n+0.5,x); %eq 4.9 %DWH eq.29
dfb=0.5*(besselj(n-0.5,x)-besselj(n+1.5,x));
dfpsi=0.5*sqrt((pi/2)/x)*besselj(n+0.5,x)+sqrt(pi*x/2)*dfb;

fpsim=sqrt(pi*(m*x)/2)*besselj(n+0.5,m*x);
fdbm=0.5*(besselj(n-0.5,m*x)-besselj(n+1.5,m*x));
fdpsim=0.5*sqrt((pi/2)/(m*x))*besselj(n+0.5,m*x)+sqrt(pi*(m*x)/2)*fdbm;

fxsi=sqrt(pi*x/2)*besselh(n+0.5,x); %eq 4.10 %DWH eq.30
fdh=0.5*(besselh(n-0.5,x)-besselh(n+1.5,x));
fdxsi=0.5*sqrt((pi/2)/x)*besselh(n+0.5,x)+sqrt(pi*x/2)*fdh;

an=(fpsi.*fdpsim-m*fpsim.*dfpsi)./(fxsi.*fdpsim-m*fpsim.*fdxsi); %eq 4.56 %DWH
eq.26
bn=(m*fpsi.*fdpsim-fpsim.*dfpsi)./(m*fxsi.*fdpsim-fpsim.*fdxsi); %eq 4.57 %DWH
eq.27
```

```
text=(l_vac/m_env)^2/(2*pi)*sum((2*n+1).*real(an+bn)); %total ext cs %eq 4.62
%DWH eq.32
tscat=(l_vac/m_env)^2/(2*pi)*sum((2*n+1).*(abs(an).^2+abs(bn).^2)); %total scat cs
%eq 4.61 %DWH eq.33
tabsorp=text-tscat; %total abs cs

theta=0:0.1:25;
fpi=zeros(length(n),length(theta));
ftau=zeros(length(n),length(theta));
mu=cosd(theta);

%calculated by the info given between eq.4.47 and 4.48
%fpi(0)=0;
%fpi(1)=1;
fpi(1,:)=1;
fpi(2,:)=3*mu;
ftau(1,:)=mu;
ftau(2,:)=6*mu.^2 - 3;

for n2=3:M
   fpi(n2,:)=(2*n2-1)/(n2-1)*mu.*fpi(n2-1,:)-n2/(n2-1).*fpi(n2-2,:); %eq 4.47
   ftau(n2,:)=n2*mu.*fpi(n2,:)-(n2+1)*fpi(n2-1,:); %eq 4.48
end

En=(2*n+1)./(n.*(n+1)); %DWH eq.22
aif0=abs(En.*an*fpi+En.*bn*ftau).^2; %DWH eq.22
aif90=abs(En.*an*ftau+En.*bn*fpi).^2; %DWH eq.23

m_air=1;
dscat0=(l_vac/m_env)^2/(4*pi^2)*aif0; % diff scat cs (parallel) %DWH eq.19
dscat90=(l_vac/m_env)^2/(4*pi^2)*aif90; % diff scat cs (perpendicular) %DWH eq.20
dscat=(dscat0+dscat90)/2; % diff scat cs (unpolarized) %DWH eq.21

theta2=asind(sind(theta)*m_env/m_air);

plim=find(theta2(:)>=5&theta2(:)<=21); %between 5-21 degree
[aa,bb]=findpeaks(dscat(plim));
peaks=round(theta2(bb+plim(1)),1); %calculation of peak angle

plot(theta2(plim),dscat(plim)./max(dscat(plim)),'LineWidth',2,'Color','r','LineStyle','-');
%title('Unpolarised');
xlabel('Scattering Angle ( ^\circ )','FontSize',16)
ylabel('Differential scattering cross section (A.U.)','FontSize',16)
xlim([theta2(plim(1)) theta2(plim(end))]); hold on
xlim([5 22])
ylim([0 1])

lmb=char(hex2dec('039B'));
fprintf(['Peaks at;\n' 'Diameter(um): ', num2str(d*1e+6), '\n' ...
        lmb '(nm): ' num2str(l_vac*1e+9) '\n' ...
```

```
'n_sphere: ', num2str(m_sph), [', and \n' ...
'n_medium: '], num2str(m_env) ' = [',num2str(peaks) ']\n']) %??
```

OUTPUT:

Peaks at;

Diameter(um): 8

Λ(nm): 656.3

n_sphere: 1.79, and

n_medium: 1.331 = [7.2 12.2 18.5]

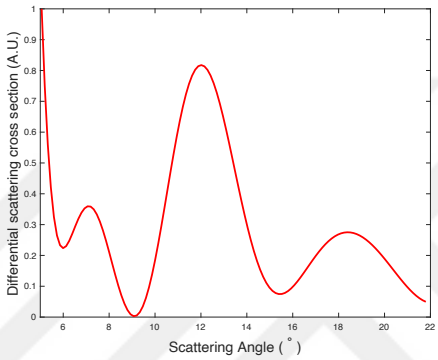

Figure A.1 Theoretical result of angular scattering of Me8 particles by 656.3 nm laser.

APPENDIX B

Code for Dataset Creation

```
clear
clc

line=0;
wl=[656.3 514.9 403.8];
rad=5:0.5:13;
nparticle=1.3:0.01:2.2;
nmed=[1.331 1.3344 1.3388];

%H20:  1.3310R, 1.3344G, 1.3388B
%ME:   1.79-R, 1.89-G, 1.96-B
%PS:   1.589-R, 1.601-G, 1.617-B

for i1=1:length(wl)
for i2=1:length(rad)
for i3=1:length(nparticle)

   line=line+1;

   [a(line,:),theta,theta2]=mie(wl(i1),rad(i2),nparticle(i3),nmed(i1));

   dta(line,1)=wl(i1);
   dta(line,2)=rad(i2);
   dta(line,3)=nparticle(i3);
   dta(line,4)=nmed(i1);


end
end
end
```

APPENDIX C

Sample dataset for Model 1

Table C.1 Sample lines from dataset adjusted for training for Model 1.

	Incident wl (nm)	n_med	p1	p2	p3	p4	d_part (µm)
1	403,8	1,3388	8,2	13,4	18,5	0,0	5
2	403,8	1,3388	8,4	13,6	18,5	0,0	5
3	403,8	1,3388	8,6	13,6	18,5	0,0	5
4	403,8	1,3388	8,6	13,6	18,5	0,0	5
5	403,8	1,3388	8,6	13,6	18,5	0,0	5
6	403,8	1,3388	8,6	13,6	18,3	0,0	5
…	…	…	…	…	…	…	…
1545	403,8	1,3388	6,6	8,2	10,1	13,3	13
1546	403,8	1,3388	6,6	8,4	12,0	15,2	13
1547	403,8	1,3388	6,7	8,3	10,6	11,4	13
1548	514,9	1,3344	10,7	17,3	0,0	0,0	5
1549	514,9	1,3344	10,8	17,5	0,0	0,0	5
1550	514,9	1,3344	11,0	17,5	0,0	0,0	5
…	…	…	…	…	…	…	…
3092	514,9	1,3344	6,1	8,2	10,8	15,2	13
3093	514,9	1,3344	6,1	8,3	10,6	14,8	13
3094	514,9	1,3344	6,0	8,4	10,2	13,0	13
3095	656,3	1,331	13,9	0,0	0,0	0,0	5
3096	656,3	1,331	14,0	0,0	0,0	0,0	5
3097	656,3	1,331	14,0	0,0	0,0	0,0	5
…	…	…	…	…	…	…	…
4636	656,3	1,331	7,7	10,4	14,3	19,2	13
4637	656,3	1,331	7,9	10,1	13,6	18,8	13
4638	656,3	1,331	7,7	13,2	17,4	0,0	13
4639	656,3	1,331	7,6	11,1	16,6	21,5	13
4640	656,3	1,331	7,6	10,7	16,1	20,2	13
4641	656,3	1,331	7,7	10,5	14,3	19,5	13

APPENDIX D

Sample dataset for Model 2

Table D.1 Sample lines from dataset adjusted for training for Model 2.

	Incident wl (nm)	n_med	p1	p2	p3	p4	n_part (um)
1	403,8	1,3388	8,2	13,4	18,5	0,0	1,30
2	403,8	1,3388	8,4	13,6	18,5	0,0	1,31
3	403,8	1,3388	8,6	13,6	18,5	0,0	1,32
4	403,8	1,3388	8,6	13,6	18,5	0,0	1,33
5	403,8	1,3388	8,6	13,6	18,5	0,0	1,34
6	403,8	1,3388	8,6	13,6	18,3	0,0	1,35
…	…	…	…	…	…	…	…
1545	403,8	1,3388	6,6	8,2	10,1	13,3	2,18
1546	403,8	1,3388	6,6	8,4	12,0	15,2	2,19
1547	403,8	1,3388	6,7	8,3	10,6	11,4	2,20
1548	514,9	1,3344	10,7	17,3	0,0	0,0	1,30
1549	514,9	1,3344	10,8	17,5	0,0	0,0	1,31
1550	514,9	1,3344	11,0	17,5	0,0	0,0	1,32
…	…	…	…	…	…	…	…
3092	514,9	1,3344	6,1	8,2	10,8	15,2	2,18
3093	514,9	1,3344	6,1	8,3	10,6	14,8	2,19
3094	514,9	1,3344	6,0	8,4	10,2	13,0	2,20
3095	656,3	1,331	13,9	0,0	0,0	0,0	1,30
3096	656,3	1,331	14,0	0,0	0,0	0,0	1,31
3097	656,3	1,331	14,0	0,0	0,0	0,0	1,32
…	…	…	…	…	…	…	…
4636	656,3	1,331	7,7	10,4	14,3	19,2	2,15
4637	656,3	1,331	7,9	10,1	13,6	18,8	2,16
4638	656,3	1,331	7,7	13,2	17,4	0,0	2,17
4639	656,3	1,331	7,6	11,1	16,6	21,5	2,18
4640	656,3	1,331	7,6	10,7	16,1	20,2	2,19
4641	656,3	1,331	7,7	10,5	14,3	19,5	2,20

APPENDIX E

Code for Random Forest algorithm

```
clear
close all
warning off
data=readtable('lib_np.xlsx');
%data2=readtable('lab_np.xlsx'); %use when lab results will be tested
prm='np'; %model type

for i=1:20
i
cv = cvpartition(size(data,1),'HoldOut',0.2); %%20 of data is separated for testing
idx = cv.test;
dataTrain=data(~idx,:);
dataTest=data(idx,:);
%dataTest=data2; %use when lab results will be tested
testing=dataTest(1:end,1:end-1);
model1=fitensemble(dataTrain,prm,'Bag',100,'Tree','Type','classification');
prediction1=predict(model1,testing);
ms1(i)=(sum(prediction1==table2array(dataTest(:,end)))/size(dataTest,1))*100;

end

accuracy=sum(ms1)/i;
sdev=std(ms1);


fprintf(['Mean of testing ' prm ' values:' num2str(mean(dataTest{:,7})) '\n']);
fprintf(['Mean of predicted ' prm ' values:' num2str(mean(prediction1)) '\n']);
```

CURRICULUM VITAE

2007 – 2012	B.Sc., Electrical & Electronics Engineering, Sakarya University, Sakarya, TURKEY
2015 – 2016	M.Sc., Electrical and Computer Engineering, Abdullah Gül University, Kayseri, TURKEY
2017 – 2020	Doctoral Candidate, Electrical and Computer Engineering, Abdullah Gül University, Kayseri, TURKEY
2023	Ph.D., Electrical and Computer Engineering, Abdullah Gül University, Kayseri, Turkey

SELECTED PUBLICATIONS AND PRESENTATIONS

J1) S. Genc, T. Erdem*, K. Icoz*, "Size, Material Type and Concentration Estimation for Micro-Particles in Liquid Samples", ACS Omega, (2023-Submitted)

J2) S. Genc, K. Icoz*, T. Erdem*, "Numerical Analysis for Size, Refractive Index, and Wavelength Dependence of Optical Scattering by Microplastics and Experimental Verification", Royal Society of Open Science, (2023-Under Review)

J3) S. Genc, M. Uguz, O. Yilmaz, E. Mutlugun*, "Rec.2100 Color Gamut Revelation Using Spectrally Ultra-Narrow Emitters", Optical Engineering, (Nov. 2017)

C1) S. Genc, K. Icoz, T. Erdem, "Machine Learning Based Classification of Microparticles Using Optical Scattering Simulations". 16th Nanoscience and Nanotechnology Conference (NANOTR), (Sept 2022).

C2) S. Genc, K. Icoz, T. Erdem, "Machine Learning Assisted Particle Size and Type Classification Using Wavelength-Dependent Scattering Patterns" International Conference on Optics and Photonics 2021 (OPTO2021), Wroclaw, Poland, Virtual Conference. (July 2021).